Arabian Journal for Science and Engineering (2023) 48:2851–2871
https://doi.org/10.1007/s13369-022-06948-6

RESEARCH ARTICLE-MECHANICAL ENGINEERING

# Effects of Fins Base Rounding on Heat Transfer Characteristics of Absorber Tube of Parabolic Trough Collector

**M. Fatouh[1,2] · Nourhan Saad[1] · Antar M. M. Abdala[1]**

Received: 17 December 2021 / Accepted: 12 May 2022 / Published online: 29 June 2022


**Abstract**
In this study, the heat transfer characteristics of an improved absorber tube of parabolic trough solar collector LS-2 are investigated using ANSYS software. Oil syltherm 800 type is used as a heat transfer fluid. Three types of absorber tubes are tested; the first is a smooth tube and the others are finned tubes. One of the rough cases is rectangular cross-section fins with rounding at fin base and the other does not have rounding at fin base. Simulations are performed with fin thickness variations of 2, 4 and 6 mm. The fin lengths change at 5, 10, 15, 20 and 25 mm. The radii of rounding are 2, 3 and 4 mm and angles between fins are 45° and 90°. Wide range of operating parameters is considered, such as inlet fluid temperatures (300:600 K), flow rate (6:24 $m^3$/h) and direct normal irradiance (500:1000 W/$m^2$). The thermal efficiency, Nusselt number and thermal enhancement index are calculated under different operating conditions. The results show that thermal enhancement index of the fin with round edge radius of 4 mm is higher than that of the fin with the sharp edge ($R = 0$ mm) by about 10.74% under the considered conditions. The thermal enhancement index of the round edge fins with a length of 25 mm is nearly 25.6% higher than that of the round edge fins with a length of 5 mm. At a fin thickness of 6 mm, the thermal enhancement index of the round edge fin is nearly 7.8% higher than that of the sharp edge fin. At 45° angle and 25-mm fin length, the thermal enhancement index for round and sharp-edged fins is 1.644 and 1.532, respectively. When the inlet fluid temperature increased from 300 to 600 K, the heat enhancement index value increased by 14.57%; as the flow rate increased from 6 to 12 m3/h, the heat enhancement index value decreased by 11.63%. The thermal enhancement index increased from 1.265 to 1.359 as the direct normal irradiance varied from 500 to 700 W/$m^2$.

**Keywords** Rectangular finned absorber · Round edge · Non-uniform heat flux · Thermal enhancement index · Pressure losses · Thermal efficiency

## List of Symbols

| | |
|---|---|
| $A$ | Area (M) |
| $C$ | Concentration ratio |
| $Cp$ | Specific heat at constant pressure (J/kg K) |
| $D$ | Diameter (m) |
| $F$ | Focal length (m) |
| $f$ | Friction factor |
| $h$ | Heat transfer coefficient (W/$m^2$K) |
| $Ib$ | Solar direct beam irradiation (W/$m^2$) |
| $K$ | Thermal conductivity (W/m.K) |
| $K$ | The incident angle modifier unity |
| $L$ | Parabola length (m) |
| $m$ | Mass flow rate (kg/s) |
| Nu | Nusselt number |
| $p$ | Fin length (mm) |
| $P$ | Pressure (kPa) |
| $Q$ | Heat flux (W) |
| Re | Reynolds number |
| $R$ | Rounding radius (mm) |
| $t$ | Fin thickness (mm) |
| $T$ | Temperature (°C) |

✉ Antar M. M. Abdala
antar451@yahoo.com

M. Fatouh
drmohfat@hotmail.com

Nourhan Saad
nourhanbahgat1992@gmail.com

[1] Faculty of Engineering, Mataria Branch, Helwan University, Cairo 11817, Egypt

[2] High Institute for Engineering, Computer Science and Administration, 1st settlement, New Cairo, Egypt

$V$ Volume flow rate ($m^3$/h)
$W$ Parabola width (m)

## Greek symbols

$\alpha$ Absorber absorbance
$\varepsilon$ Emittance
$\Delta$ Difference
$\eta_{op}$ Optical efficiency
$\eta_{th}$ Thermal efficiency
$\theta$ Angle between fins (°) (°)
$\mu$ Dynamic viscosity (Pa s)
$\rho$ Density (kg/$m^3$)
$\tau$ Transmittivity

## Subscripts

$a$ Aperture
fm Mean fluid
in Inlet
loss Thermal loss
out Outlet
$r$ Receiver
ri Inner receiver
ro Outer receiver
$s$ Solar
$u$ Useful
0 Smooth absorber (reference case)

## 1 Introduction

Parabolic trough solar collectors (PTSCs) are technologies currently used in various applications such as power generation, water distillation, air heating systems, industrial process heat generation, air conditioning and refrigeration [1]. It consists of an absorber tube inside an evacuated glass chamber. Absorber tubes are typically made of stainless steel with a spectrally selective surface coating that maximizes the absorption of solar radiation and reduces heat loss by emitting less radiation. A heat transfer fluid (HTF) circulates in an absorber tube located at the focal length and is then pumped through a series of heat exchangers to generate heat in a temperature range of 200–400 °C for a variety of applications. In order to improve the thermal performance of the PTSC, the useful heat rate has to increase for a given solar heat rate [1]. The useful heat rate can be increased by increasing the convective heat transfer coefficient within the absorber tube, or/and increasing the convective surface area within the absorber tube [2–8]. Many investigations were carried out on improved geometric designs of absorber tubes to increase their convective heat transfer and convective surface area. The current work deals with the use of extended surfaces as a passive enhancement method. Extended surfaces (fins) are surfaces that extend from the absorber tube wall to increase the rate of heat transfer from the heated surface to the heat transfer fluid. Therefore, fins are a heat transfer enhancement method that is widely used to increase the convective heat transfer rate, which depends on the surface area of the fins.

Various types of fins, such as flat longitudinal fins, wavy longitudinal fins, pin fins, and porous fins, have been studied by many researchers. Kursun [9] investigated the effect of internal longitudinal fins with flat and sinusoidal lateral surfaces on the thermal performance of receiver tubes. Their results revealed that the highest increases in Nusselt number were 25% and 78% for flat and sinusoidal fins, respectively.

Bellos et al. [10] evaluated the use of internal finned absorber tubes with sharp edges in the LS-2 PTSC. They tested different fin configurations. Their results confirmed that the optimal fin design was an absorber with a fin length of 10 mm and a fin thickness of 2 mm. With this configuration, the thermal efficiency is increased by 0.82%, the Nusselt number is increased by 65.8%, and the friction factor and pressure loss are doubled compared to the smooth tube. These results are consistent with the simulation results of Bellos et al., [11].

The number and location of internal longitudinal fins inside the absorber tube were optimized by Bellos et al. [12]. This study was performed using Syltherm 800 as the working fluid at a constant flow rate of 150 L/min. They concluded that the best designs included three fins in the lower part, resulting in a 0.51% increase in thermal efficiency. Theoretical and experimental studies have been reported to investigate the performance of multi-fin arrays [13]. The results showed that the efficiency of the half-tube fins is about 14% higher than that of the smooth absorber.

Nemś and Kasperski [14] conducted an experimental investigation, and they found a maximum efficiency of 42% in twice-daily performance evaluation tests. Amina et al. [15] studied the effect of heat transfer performance with and without fins of different shapes (triangular and rectangular). The results showed that the Nusselt number with fins was 1.3–1.8 times higher than that of the smooth tube. Laaraba and Mebarki [16] studied an internally finned absorber, the LS-2 PTSC, with fins in the lower half of the absorber tube and a total of 5 fins with varying thickness and length. They showed that by modifying the surface in this way, the thermal enhancement index can be increased to 1.6.

Using air as the working fluid, experiments were conducted on the internal pin–fin absorber tube of PTSC by Zhao et al., [17]. The experimental results showed that over the range of air flow rate from 50 to 120 $m^3$/h, the

energy efficiency of the internally pin finned was found to be 10.4–14.5%.

Gong et al., [18] investigated the heat transfer performance of an absorber tube with a pin fin for a PTSC system. They added a pin fin to the lower circumference of the absorber tube to improve thermal performance and reduce pressure drop. They reported that the heat transfer performance of PTSC with various numbers of pin fins was better than that of the plain PTSC in all cases when Re number was less than 9107.2.

Numerical studies were carried out for four configurations (circular, triangular, square, and trapezoidal) [19]. The results showed that the trapezoidal fins increased the heat transfer rate by 13.8%. In another investigation, Huang et al., [20] compared the effect of helical fins with protrusions or dimples on heat transfer enhancement in the LS-3 PTSC receiver tube. The Reynolds number was changed from $1 \times 10^4$ to $2 \times 10^4$. The realizable k-ε model was also used at the turbulent flow. The heat transfer was improved as the depth, pitches, and number of dimples were increased. They determined that the pitted receiver tube had the best thermal performance compared to the other cases. An improved absorber with hinged vanes was experimentally investigated and compared to the conventional absorber by Kalidasan et al., [21]. They found that the average efficiencies of the modified and conventional absorber tubes were 69.33% and 60.82%, respectively.

Huang et al., [22] conducted a numerical study on the effect of pit depth and heat flux distribution around receiver tubes in PTSCs. They used values of $\mathrm{Re} = 2 \times 10^4$ and $0 \leq \mathrm{Gr} \leq 3.2 \times 10^{10}$. They also used the k-ε turbulence model and the Boussinesq approximation. They reported that the effect of natural convection from a non-uniform heat flux distribution around the receiver tube is greater than that of a uniform heat flux distribution. The thermal efficiency ($\eta$) of the tube under non-uniform heat flux was changed from 1.05 to 1.06 for shallow dimples of 1 mm depth and 1.31–1.34 for deep dimples of 7-mm depth at $\mathrm{Gr} = 10^9 - 3.2 \times 10^{10}$. Bellos et al. [23] used a converging–diverging absorber tube shape to work with thermal oil, and concluded that thermal efficiency was improved by an average of 4.25%. Demagh et al. [24] studied a sinusoidal absorber that, when used with Syltherm 800, provided a 3% increase in thermal efficiency and a 50% increase in pressure drop.

Fuqiang et al., [25] conducted a numerical study on the heat transfer performance and thermal strain of a symmetrically convex corrugated absorber tube in a PTSC system. Corrugated tubes increased the rate of heat transfer by breaking the momentum and thermal boundary layers.

In their study, they used the usual k-ε model and the MCRT method. The Reynolds numbers were between 15,000 and 90,000, and the corrugation spacing $p/D$ values were 4.3, 6.3, 9.4, and 14. With the decrease in $p/D$, the maximum thermal strain on the absorber tube was lowered.

The Nusselt value increases with decreasing p/D due to the increased corrugation zone. Using a symmetrically convex corrugated absorber tube with $\mathrm{Re} = 81{,}728$ and $p/D = 4.3$, the thermal performance ($\eta$) was increased to 8.4%.

Mahmoud et al., [26] conducted a numerical study of the conical pin–fin arrangement in a parabolic trough tube. The results showed an average enhancement rate of 56.2% was achieved for fin heights from 2 to 12 mm. Okonkwo et al., [27] carried out a comparison between four geometry configurations of absorber tubes (smooth absorber tube, internally finned absorber tubes, convergent–divergent absorber tube and absorber tube with twisted tape) at various range of inlet fluid temperature of 300–600 K and flow rate with range of 40–200 l/min. They found that the best geometry was a convergent adiabatic absorber tube with a thermal efficiency of 65.95% at an inlet fluid temperature of 600 K and a flow rate of 200 l/min.

Okonkwo et al. [28] presented a comparative study of heat transfer characteristics in parabolic trough collectors with modified in absorber tubes (twisted tape inserts, internally finned absorber, porous insert, and convergent–divergent absorber tube) at different levels of inlet fluid temperature and flow rate with 300–600 K and 20–100 l/min, respectively. The results showed that the convergent–divergent absorber tube provides a maximum thermal enhancement of 1.16% at 600 K and a flow rate of 100 l/min.

Bellos and Tzivanidis [29] used an engineering equation solver to evaluate the performance of parabolic trough solar collectors with different configurations of non-evacuated receivers (twisted ribbon inserts, perforated plates, and internally finned absorbers). Their results showed that the internal finned absorber achieved the highest thermal enhancement index of 1.6%.

Khan et al., [30] conducted a numerical investigation using an engineering equation solver to compare the thermal efficiency of absorbers with different geometries (smooth tubes, internal fins, and twisted-belt inserts). They found that the best thermal efficiency of 72.10% was achieved using internal fins.

Various studies on the addition of nanoparticles to the working fluid of solar collectors [31–40] have improved the thermal conductivity and thus the thermal performance of these collectors. Bellos et al. [41] investigated the effect of oil-based nanofluids (6% Cuo) with internal fins on heat transfer characteristics. The results showed that the improved thermal efficiencies of nanofluid, inner fin and both are 0.76%, 1.1% and 1.54%, respectively. Bellos et al., [42] investigated the influence of multiple cylindrical longitudinal inserts in a parabolic trough collector. They found a 0.656% increase in thermal efficiency of the four blades.

Akbarzadeh and Valipour [43] reviewed the effect of various parameters on the thermal performance. Ahmed and Natarajan [44] studied the effect of toroidal rings on heat

transfer performance. The results showed that the thermal efficiency is improved by 3.74%. Vishwakarma et al. [45] conducted a numerical study on the heat transfer of four different types of helical groove absorber tubes (semicircular, rectangular, trapezoidal and triangular) under solar radiation of 818.5 W/m$^2$ and Re of 4000. Their results proved that the best geometry was a triangular absorber tube with a Nusselt number of 85.49. Amani et al. [46] studied the influence of conical strip inserts on the thermal performance of a parabolic trough collector at an inlet fluid temperature of 300 K and different Re (8000–40,000) levels. The results showed that the Nusselt number increased by 91.949%. Okonkwo et al. [47] demonstrated the influence of converging–diverging absorber tubes for six different working fluids. Their results showed that the thermal efficiency is increased by about 1.13%.

Singh and Dhiman [48] investigated a rectangular longitudinal fin solar air heater with a semicircular absorber plate with a Re range of 1600–4300. The results revealed that the double-glazed cover and cyclic operation improve thermal performance. Kalidasan et al., [49] conducted internal pin–fin experiments in the absorber tube of a parabolic trough collector. They found that the thermal efficiency of the inner finned tubes reached 36.89%.

Ganga and Jacob [50] performed a numerical investigation of turbulent flow in a staggered pin–fin arrangement in a receiver tube. Their results showed that heat transfer increases with increasing pin–fin height due to the increased contact area between the working fluid and the inner wall.

Biswakarma et al. [51] conducted a numerical analysis of the performance improvement of a parabolic trough collector with an internal helical V-groove for solar radiation ranging from 600 to 1000 W/m$^2$ with Re ranging from 4000 to 6000. The results showed that when the solar radiation is 1000 W/m$^2$ and Re is 6000, the heat transfer coefficient increases by 41.3%. Zaboli et al. [52] numerically analyzed absorber tubes with internal helical axial fins, considering swirl generators or turbulators. This technology improves thermal performance by 23.1%.

Nnamchi et al. [53] presented data revealing an innovative design of a parabolic trough solar collector (PTSC). The design equations were formulated on the optical and thermal principles using rim angle, optical efficiency, aperture and concentration ratio. Sharma and Jilte [54] conducted a review of geometrical modification of receiver tube that used to enhance heat transfer characteristics.

The literature review indicates that the internal longitudinal fins are considered as an efficient technique to enhance heat transfer characteristics. Many researchers have predicted the effects of fin thickness (2 and 4 mm), fin length (5–20 mm) and fin angle of 45° on the heat transfer and pressure drop characteristics of PTSC absorber tubes. Most of the work done on the inner longitudinal fins was carried out under specific operating conditions, namely a flow rate of 9 m$^3$/h, a working fluid inlet temperature of 600 K, and a direct solar radiation intensity of 1000 W/m$^2$. As reported in the literature, little work has been done within a narrow range of flow rates, working fluid inlet temperatures, and solar radiation intensity. To date, no significant studies have been published on longitudinal fins with rounded edges inside PTSC absorber tubes.

The objective of the present work is to compare the rounded and sharp edges of flat longitudinal fins of different radii (2–3–4 mm), length (5–10–15–20–25 mm), thickness (2–4–6 mm), angle between fins (45°–90°). Also, the effects of working fluid inlet temperature (300–600 K), flow rate (6–24m$^3$/h) and solar radiation (500–1000 W/m$^2$) on the heat transfer characteristics and pressure drop through the PTSC absorber need to be predicted. To achieve this objective, a simulation model was developed with commercial ANSYS software, and the developed simulation model was validated with experimental data from the literature. The thermal performance and pressure drop of smooth, sharp finned and round edge finned absorber tubes were compared across the considered range of geometric and operating parameters.

## 2 Physical Model

Figure 1 shows the main parts of a standard LS-2 parabolic trough concentrator, which is used in the current work. The standard parabolic trough collector consists of a reflector (linear parabolic mirror) and an evacuated tube (receiver). The reflector has a reflectivity of 0.83, while the evacuated tube includes a stainless steel absorber and glass cover. The absorber tube had an inner diameter of 66 mm and an outer diameter of 70 mm, and the surface absorption rate ($\alpha$) was 0.96. The glass cover has an inner diameter of 109 mm and an outer diameter of 115 mm, with a transmittance ($\tau$) of 0.95 and an emissivity ($\varepsilon$) of 0.86 [55]. PTCs use direct solar radiation, called direct normal irradiance (DNI), which comes directly from the sun. A linear parabolic mirror reflects and concentrates the received solar energy onto a receiver positioned along the focal line of the PTC, as shown in Fig. 1. Incident rays are collected by the receiver tube, which converts it into heat, which is carried by the heat transfer fluid through the absorber tube. As shown in Fig. 2, the focal length of the LS-2 parabolic trough module is 1.84 m, and the width and length of the parabola are 5 m and 7.8 m, respectively; then the total aperture area ($A_a$) is 39m$^2$ and concentration ratio ($C = A_a/A_{r,o}$) is 22.74.

Due to various optical losses such as tracking errors and possible manufacturing errors, the final optical loss value reported by Behar et al. [56] is 0.755. Details of the LS-2 parabolic trough can be found in the literature [57]. The model is simplified by assuming the incident angle is

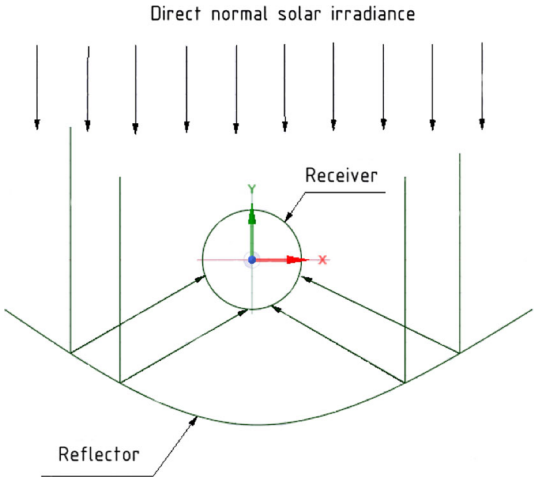


**Fig. 1** Schematic diagram of a solar parabolic trough concentrator

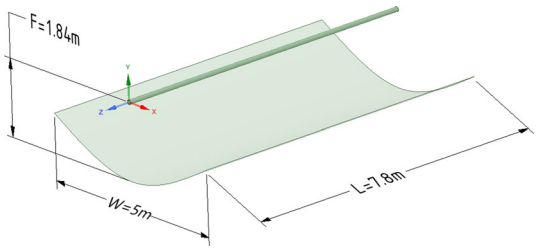


**Fig. 2** Standard LS-2 parabolic trough concentrator

zero, vacuum pressure in the glass envelope, and radiation exchange between the absorber surface and the glass envelope is almost negligible.

The present work aims to improve the heat transfer characteristics of PTC absorber tubes using turbulators with internal rectangular longitudinal fins with rounded edges of different radii (2–3–4 mm), length (5–10–15–20–25 mm), thickness (2–4–6 mm), angle between fins (45°–90°) as shown in Fig. 3. Also, it is necessary to investigate the effect of the working fluid inlet temperature (300–600 K), flow rate (6–24 $m^3$/h) and solar radiation (500–1000 W/$m^2$) on the heat transfer characteristics and pressure drop through the absorber tube of PTSC.

## 3 Simulation Model

The governing equations for the conservation of mass (Eq. 1), conservation of momentum (Eq. 2), and conservation of energy (Eq. 3) are used to model the performance characteristics of the absorber tube in a standard parabolic trough collector.

$$\frac{\partial}{\partial x_i}(\rho u_i) = 0 \tag{1}$$

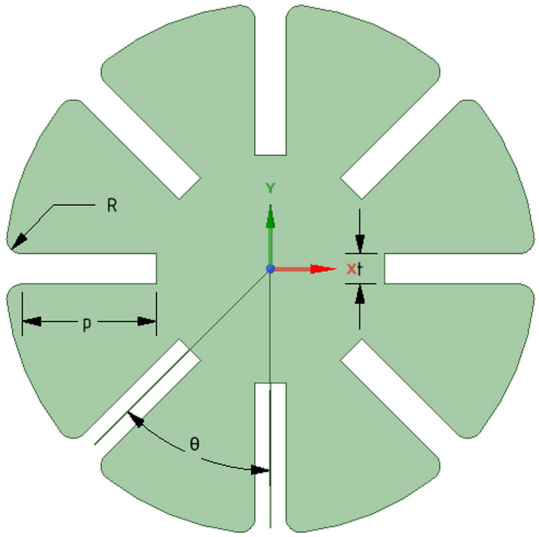


**Fig. 3** Internally rectangular longitudinal fins with round edge shape (present model)

$$\frac{\partial}{\partial x_i}(\rho u_i u_j) = -\frac{\partial p}{\partial x_i} + \frac{\partial}{\partial x_j}\left[\mu\left(\frac{\partial u_i}{\partial x_j} + \frac{\partial u_j}{\partial x_i}\right) - \frac{2}{3}\mu\frac{\partial u_i}{\partial x_i}\delta_{ij} - \rho u_i u_j\right] \tag{2}$$

$$\frac{\partial}{\partial x_j}\left(\rho u_j c_p T\right) = \frac{\partial}{\partial x_j}\left(\lambda\frac{\partial T}{\partial x_j} + \frac{\mu_T}{\sigma_{h,T}}\frac{\partial\left(c_p T\right)}{\partial x_j}\right) + \left[\mu_j\frac{\partial P}{\partial x_j} + \mu\left(\frac{\partial u_i}{\partial x_j} + \frac{\partial u_j}{\partial x_i}\right) - \frac{2}{3}\mu\frac{\partial u_i}{\partial x_i}\delta_{i,j} - \rho u_i u_j\right]\frac{\partial u_i}{\partial x_j} \tag{3}$$

where $u_i$ and $u_j$ are the time-averaged velocity components in the $i$ and $j$ directions, $\rho u_i u_j$ are the Reynolds stresses, $P$ is the time-averaged pressure, $T$ is the time-averaged temperature, $\lambda$ is the fluid thermal conductivity, $\rho$ is the density, $\mu_t$ is the turbulent viscosity and $\sigma_{h,T}$ is the turbulent Prandtl number for energy. The Reynolds stresses can be expressed by the following equation depending on the Boussinesq hypothesis to include velocity gradients [58],

$$\rho u_i u_j = \mu\left(\frac{\partial u_i}{\partial x_j} + \frac{\partial u_j}{\partial x_i}\right) - \frac{2}{3}\mu\left(\rho k + \mu_t\frac{\partial u_k}{\partial x_k}\right)\delta_{ij} \tag{4}$$

where $\delta_{ij}$ is the linear deformation rate of a fluid element, $k$ is the turbulent kinetic energy per unit mass.

$\delta_{ij}$ and k are given by Eqs. 5 and 6,

$$\delta_{ij} = \frac{1}{2}\left(\frac{\partial u_i}{\partial x_j} + \frac{\partial u_j}{\partial x_i}\right) \tag{5}$$

$$k = \frac{1}{2}(u^2 + v^2 + w^2) \tag{6}$$

For the $k-\varepsilon$ realizable model, the kinetic energy $k$ is given by the expression and turbulent dissipation rates ($\varepsilon$) are given

by Eqs. 7 and 8,

$$\frac{\partial}{\partial x_j}(\rho k u_j) = \frac{\partial}{\partial x_i}\mu\left[\left(\mu + \frac{\mu_t}{\sigma k}\right)\frac{\partial k}{\partial x_j}\right] + G_k - \rho\varepsilon \tag{7}$$

$$\frac{\partial}{\partial x_j}(\rho\varepsilon u_j) = \frac{\partial}{\partial x_i}\mu\left[\left(\mu + \frac{\mu_t}{\sigma\varepsilon}\right)\frac{\partial \varepsilon}{\partial x_j}\right] + \rho C_1 S_\varepsilon - \rho C_2 \frac{\varepsilon^2}{k + \sqrt{v\varepsilon}} \tag{8}$$

where $\sigma k$ and $\sigma\varepsilon$ are the turbulent Prandtl number for $k$ and $\varepsilon$, respectively. $G_k$ is the production of turbulent kinetic energy and $\mu_t$ is the turbulent viscosity are given by the expression 9 and 10,

$$G_k = \mu_t S^2 \tag{9}$$

$$\mu_t = \rho C_\mu \frac{k^2}{\varepsilon} \tag{10}$$

Constants used in the realizable k-ε model are given below:

$$C_1 = \max\left[0.43, \frac{\frac{\mathrm{Sk}}{\mathrm{n}}}{5 + \frac{\mathrm{Sk}}{\mathrm{n}}}\right], \mathrm{S} = \sqrt{\mathrm{S_{ij}S_{ij}}}, \mathrm{C_2} = 1.9, \mathrm{sk} = 1, \mathrm{s''} = 1.2$$

$C_\mu$ is a function of the mean strain and rotation rates, the angular velocity, and the turbulence fields.

Calculation of $C_\mu$ function is given in reference [58].

These governing equations are modeled by Reynolds-averaged Navier–Stokes (RANS) equations, which are based on a finite governing volume approach and employ a structured mesh to achieve high nodal resolution. The 3D model is developed using ANSYS software with two user-defined functions (UDFs). These two UDFs are used to calculate the heat flux wall boundary condition for the tube wall using the input solar flux. These governing equations are solved in each cell at steady-state condition in the incompressible fluid domain with turbulent flow under the range of investigated parameters of inlet water temperature, velocity, and heat flux. The steady, pressure-based coupled algorithm method is used to solve the problem as it obtains more robust and efficient single-phase implementation for steady-state flows. Least squares cell-based is used for gradient, second-order upwind discretization is used for energy and momentum, and second order is used for pressure to control the spatial discretization of the convection terms in the equations. The pseudo-transient helps to stabilize the case and at the same time, gives faster convergence. The correct simulation depends on the appropriate specifications of the boundary conditions. Each simulation is assumed to converge when the residuals for the energy equation are less than $10^{-6}$ and those for the equations of continuity and momentum are less than $10^{-4}$.

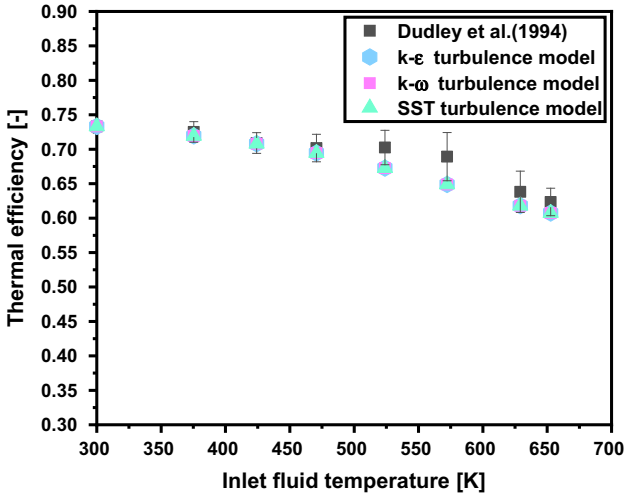


**Fig. 4** Comparison between three turbulence models and experimental results to select the best turbulence model

**Table 1** Boundary condition of the present work

| Boundary condition | Values |
|---|---|
| Inlet | The inlet temperature, $T_{in}$ (300:600) K<br>The volume flow rate, $V$ (6:24) $m^3/h$ |
| Outlet | Fully developed flow and zero pressure gauge |
| Outer wall | Non-uniform heat flux with DNI (500:1000) $W/m^2$ |

The present fluid domain was validated by Dudley et al., [57] using three different turbulence models, $k-\varepsilon$, $k-\omega$, and SST as shown in Fig. 4. The average deviations of the thermal efficiencies for the turbulent $k-\varepsilon$, $k-\omega$ and SST models are 2.740%, 2.737% and 2.736%, respectively, the computation times are 8 h, 11 h, and 12 h, respectively. Therefore, the turbulence model suitable for the current fluid domain is the realizable k-ε model because of its short computation time.

## 4 Mathematical Model and Boundary Conditions

### 4.1 Boundary Conditions

The inlet boundary conditions are the flow rate and the inlet temperature of thermal oil, as listed in Table 1. The outlet is fully developed flow. Thermal oil is used as a heat transfer

fluid in present work and its properties are reported in the literature [57].

### 4.2 Mathematical Model

Thermal efficiency ($\eta_{th}$) and thermal enhancement index (TEI) are the two main important considerations when comparing different configurations of finned absorber tube versus smooth absorber tube for a solar PTC.

The thermal efficiency $\eta_{th}$ of a solar collector is defined as the ratio of the useful heat rate ($Q_u$) to the available solar irradiation ($Q_s$), i.e.,

$$\eta_{th} = \frac{Q_u}{Q_s} \tag{11}$$

The useful heat rate ($Q_u$) captured by the fluid is calculated from the energy balance over the fluid control volume. It is given in the following expression:

$$Q_u = \dot{m} \cdot c_p \cdot (T_{\text{out}} - T_{\text{in}}) \tag{12}$$

where $\dot{m}$ is the mass flow rate of working fluid, $c_p$ is the specific heat of working fluid, Tin is the inlet temperature of working fluid, and Tout is the outlet temperature of the working fluid and it is known by the computational tool. The solar radiation (Qs) received by the solar collector can be determined as the product of the solar beam radiation (Ib) and the reflector aperture area (Aa) as shown in the following equation:

$$Q_s = Aa.Ib \tag{13}$$

It can be said that the value of Ib is 1000 W/m$^2$, and the reflector aperture area is 39 m$^2$. Therefore, the available solar radiation at the collector aperture is 39000 W.

A further point to consider is the Thermal Enhancement Index (TEI), which considers the Nusselt enhancement in addition to the increase in the coefficient of friction. This index is the main factor for comparing the different configurations of finned absorber tubes and smooth absorber tubes. It can be expressed as:

$$\text{TEI} = \frac{\text{Nu}/\text{Nu}_0}{\left(\frac{\text{f}}{\text{f}_0}\right)^{1/3}} \tag{14}$$

where Nu is the Nusselt number of the finned absorber tube, $\text{Nu}_0$ is the Nusselt number of the smooth absorber tube, $f$ refers to the friction factor of the finned absorber tube and $f_0$ represents the friction factor of the corresponding reference case. When TEI is over 1, then the examined case is better thermal performance compared to the respective reference case.

The Nusselt number (Nu) depends on the geometry of the absorber tube and flow conditions. It can be calculated as follows:

$$\text{Nu} = \frac{\text{h.D}_{\text{ri}}}{\text{K}} \tag{15}$$

where k is the thermal conductivity of the working fluid and Dri is the inner diameter of the absorber tube, which varies with fin geometry and h is the convective heat transfer coefficient between the absorber tube and the working fluid, which can be calculated by Eq. (16).

$$h = \frac{Q_u}{(\text{ß.D}_{\text{ri}}.\text{l}).(T_r - T_{fm})} \tag{16}$$

In the above equation, the useful heat ($Q_u$) is calculated by Eq. (12), the average temperature of the receiver ($T_r$) is known by the computational tool, the average fluid temperature ($T_{fm}$) is calculated by Eq. (17), and $l$ and $D_{ri}$ are the length and diameter of the absorber tube, respectively.

$$T_{fm} = \frac{(T_{\text{in}} + T_{\text{out}})}{2} \tag{17}$$

The friction factor ($f$) is calculated using the pressure losses ($\Delta$p) along the absorber tube, using the following equation:

$$\text{f} = \frac{1\text{p}.1000}{\frac{1}{2}.\text{æ}.\text{u}^2}.\left(\frac{\text{D}_{\text{ri}}}{\text{l}}\right) \tag{18}$$

where $\rho$ is the density of the working fluid and $u$ is the average velocity of the working fluid. It can be stated that the pressure losses $\Delta p$ [kPa] along the absorber tube are known by the computational tool.

## 5 Meshing and Model Validation

### 5.1 Mesh Independent Study

ANSYS software (mesh) is used to create the mesh required for the current study, and the domains are hexahedral elements. Mesh quality is evaluated by aspect ratio, skewness, and orthogonal quality. The edge sizing is used as the rounded edge of the rectangle of the heat transfer oil domain and create ten expansion layers on the walls of the liquid domain with a growth ratio of 1.2 and a maximum thickness of $4 \times 10^{-5}$ m. The constructed mesh provides an aspect ratio smaller than 5; skewness ranges from 0 to 0.5; and orthogonal quality ranges from 0.5 to 1.

The grid independence verification test is performed on six different numbers of grid cells 300,000, 600,000, 800,000, 1,076,400, 2,630,880 and 3,700,000 as shown in Fig. 5.

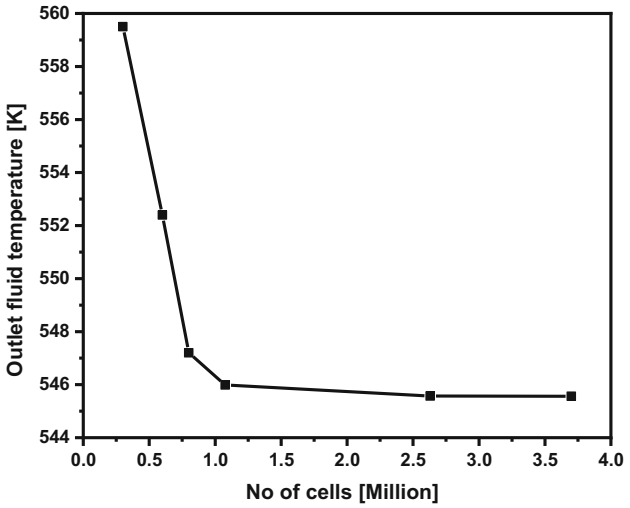


**Fig. 5** Variation of outlet fluid temperature with number of cells

Clearly, the outlet fluid temperature keeps almost constant when the number of cells reaches 2,630,880.

Therefore, a mesh size of 2,630,880 provides accurate results and reasonable computation time and is used throughout the validation and the present work.

To show the error ratio between the simulation values of heat transfer fluid's outlet temperature and the experiment [57], Table 2 is used. Clearly, the mesh size of 2,630,880 produces accurate results as given in Table 2.

Figure 6 shows a 3D view of the structured hexahedral mesh used for the final meshing of the absorber tubes in the current study.

## 5.2 Model Validation

The simulation model is validated against the experimental data reported by Dudley et al. [57] for the smooth absorber tube. Figure 7 shows a comparison between the experimental thermal efficiency data from Dudley et al. [57] and thermal efficiency data for the present model of the smooth absorber tube. It is found that the average deviation is relatively low, about 2.74%.

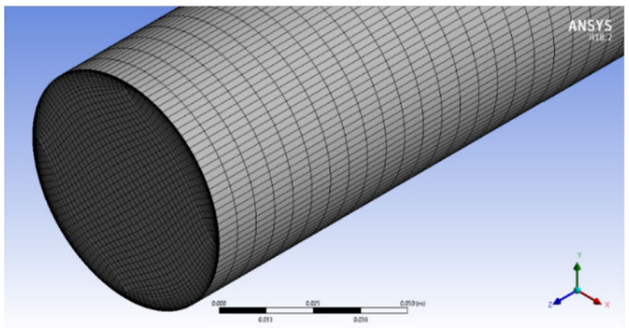


**Fig. 6** Three-dimensional view of structured hexahedral mesh for final meshing of absorber tube

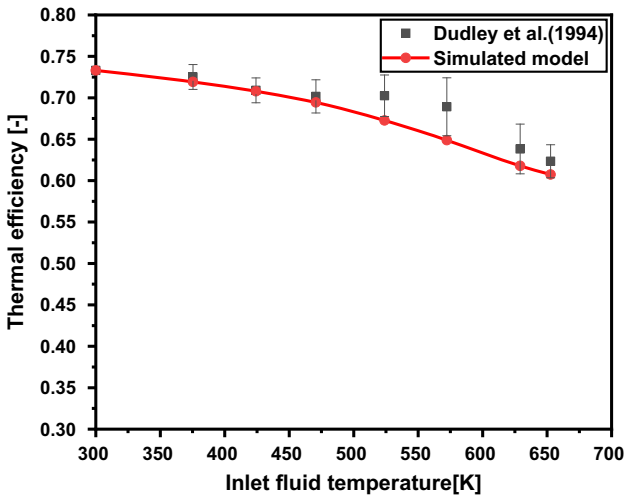


**Fig. 7** Comparisons between the present model and experimental results for validation

# 6 Results and Discussion

## 6.1 Effect of Radius of Round Edge

Influence of round edge radius ($R$) on thermal performance characteristics at fin length of 20 mm, fin thickness of 4 mm, fluid inlet temperature of 600 K, and fluid flow rate of 9 $m^3$/h and direct normal irradiance of 1000 W/$m^2$ is presented and discussed below.

The distribution values of the receiver temperature with the angle of the peripheral absorber under different radii are shown in Fig. 8a. Clearly, the smooth absorber tube has the

**Table 2** Grid independence tests

| Parameter | Mesh1 | Mesh2 | Mesh3 | Mesh4 | Mesh5 | Mesh6 |
|---|---|---|---|---|---|---|
| No of cells | 300,000 | 600,000 | 800,000 | 1,076,400 | 2,630,880 | 3,700,000 |
| $T_{out}$ (sim) | 559.5 | 552.4 | 547.2 | 545.99 | 545.575 | 545.569 |
| $T_{out}$ (EXP) | 542.6 | 542.6 | 542.6 | 542.6 | 542.6 | 542.6 |
| Error % | − 3.12 | − 1.81 | − 0.85 | − 0.624 | − 0.548 | − 0.547 |

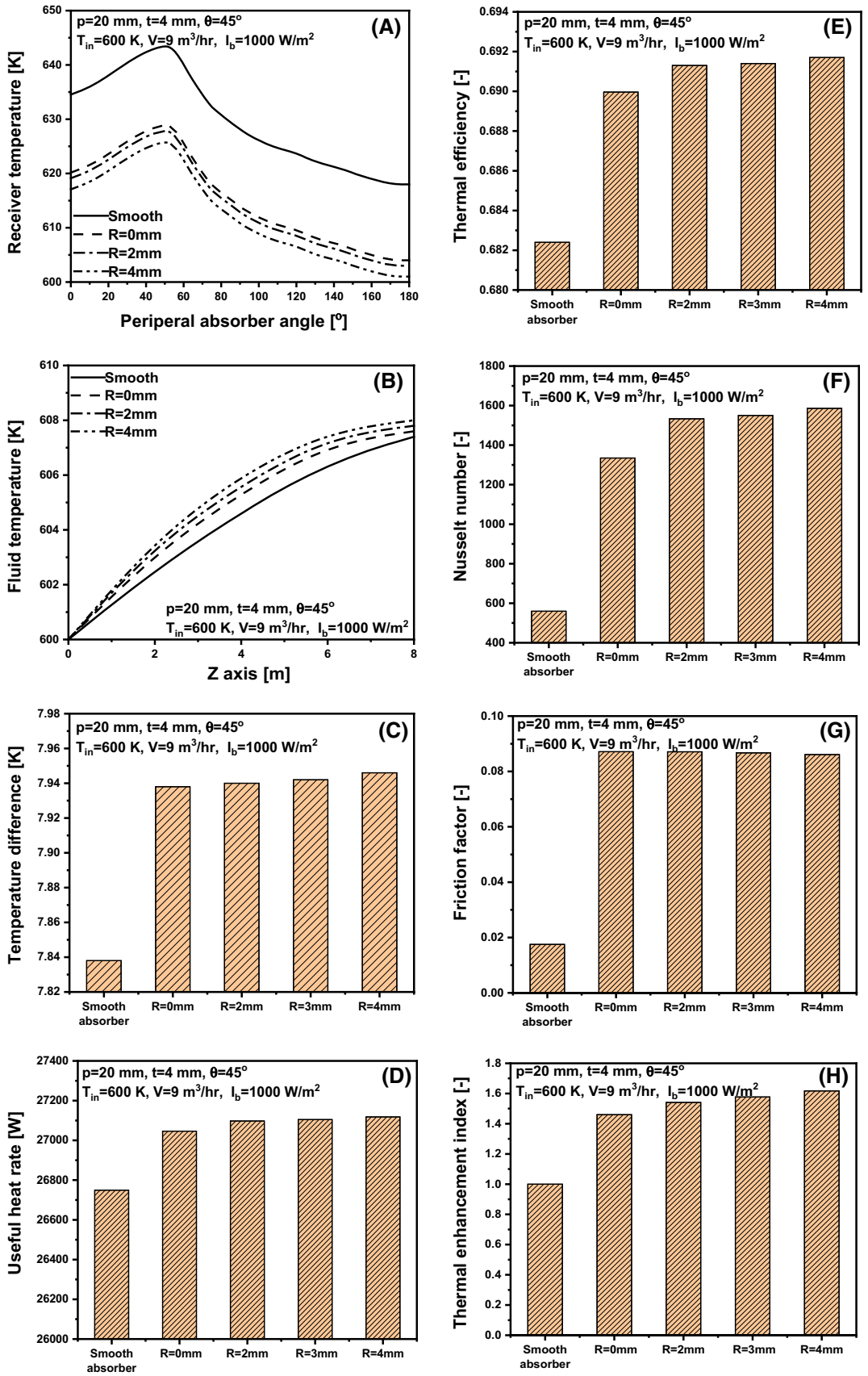


**Fig. 8** Effect of radius of round edge on heat transfer characteristics

highest temperature level over the peripheral absorber tube, while the finned absorber tubes with both the sharp edge ($R = 0$ mm) and the round edge ($R = 2$ and 4 mm) have lower temperature levels over the peripheral absorber compared with the smooth absorber tube. The maximum and minimum temperatures at $R = 4$ mm are 625.61–643.2 K and 601.11–618.21 K for the smooth and round finned cases, respectively. The results show that the round finned case reduces the absorber temperature, thereby reducing heat loss and increasing the useful heat, thereby improving thermal efficiency.

The relationship between the outlet fluid temperature value and different radii is shown in Fig. 8b. The results show that the highest outlet temperature is achieved with the finned absorber. In the cases considered, the outlet fluid temperature of the round finned absorber is the highest.

The temperature difference between the outlet and inlet fluid temperatures at different radii is shown in Fig. 8c. It is indicated that the temperature difference of the round finned absorber at $R = 4$ mm is about 1.38% higher than that of the smooth absorber.

Useful heat rate values are shown in Fig. 8d for smooth absorbers and rounded finned absorbers of different radii. The useful heat rate increases with the radius of the rounded edge, as it creates higher turbulence in the fluid flow and increases the heat transfer rate inside the flow. It can be seen that the round edge radius of 4 mm yields the largest useful heat rate. In this case, the useful heat rate is increased by about 1.4% compared to the smooth absorber.

Figure 8e illustrates the thermal efficiency of smooth absorber tubes and finned absorber tubes with different rounded edge radii. The larger the rounded edge radius, the higher the thermal efficiency because it has higher useful heat for the same direct solar irradiance. As shown in Eq. (11), thermal efficiency has similar behavior to useful heat. The thermal efficiency of the round finned absorber with $R = 2$ mm is nearly 1.3% higher than that of the smooth absorber.

The Nusselt number as a function of different radii for rounded edge absorber and smooth absorber is shown in Fig. 8f. Clearly, the highest Nusselt number is achieved using the maximum radius of the rounded fins. The Nusselt number of the rounded fins with a radius of 4 mm is nearly 1.2 times that of the sharp-edged fins ($R = 0$ mm).

The friction factor for the absorber tube case considered is shown in Fig. 8g, which confirms that the friction factor for fins with rounded edges ($R = 4$ mm) and fins with sharp edges ($R = 0$ mm) are 0.0861 and 0.08714, respectively.

The thermal enhancement index for the considered cases is shown in Fig. 8h. Clearly, the thermal enhancement index increases when the radius of the rounded edge of the fin increases. The thermal enhancement indices were 1.617, 1.577, 1.541 and 1.4601 for $R = 4$ mm, $R = 3$ mm, $R = 2$ mm and $R = 0$ mm, respectively. Consequently, thermal enhancement index of the fin with round edge radius of 4 mm is higher than that of the fin with the sharp edge ($R = 0$ mm) by about 10.74% under the considered conditions. This means that the suitable case to achieve the higher thermal enhancement index is $R = 4$ mm.

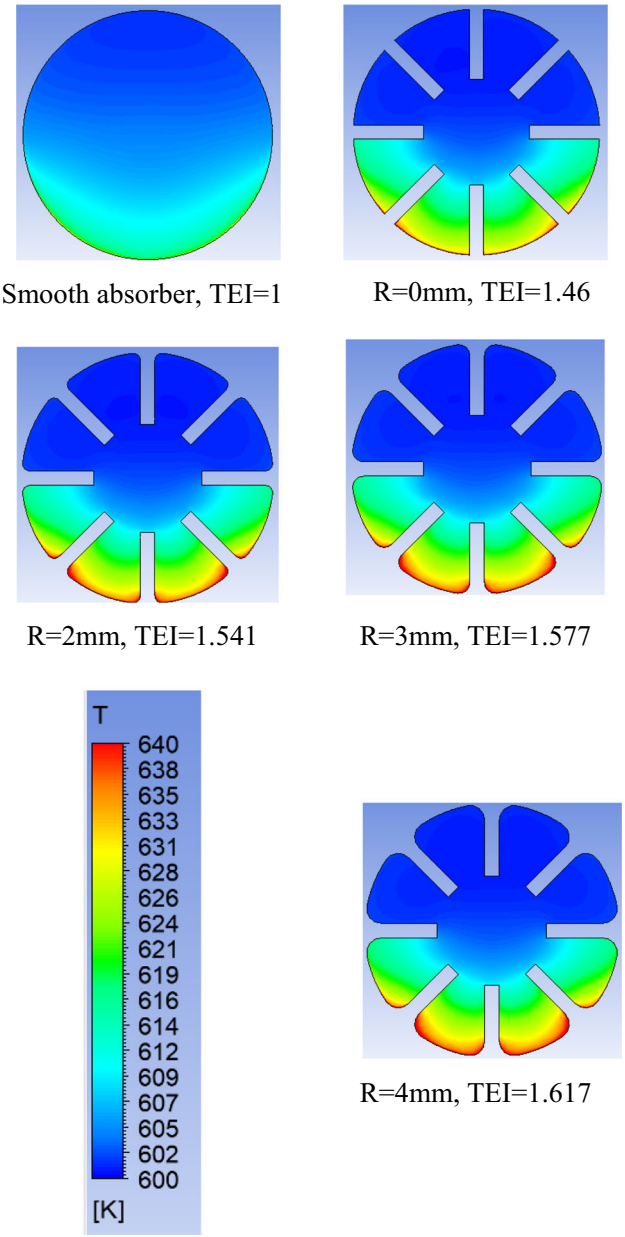


**Fig. 9** Temperature distribution contours in a mid-length of absorber tube for different radii

The contours of the temperature distribution in the middle section of the absorber tube with different radii are shown in Fig. 9. It is obvious that the temperature of the fluid in round finned absorber is higher than that in smooth absorber and the sharp edge case ($R = 0$ mm) due to the higher heat transfer that creates in the round finned absorber, as shown

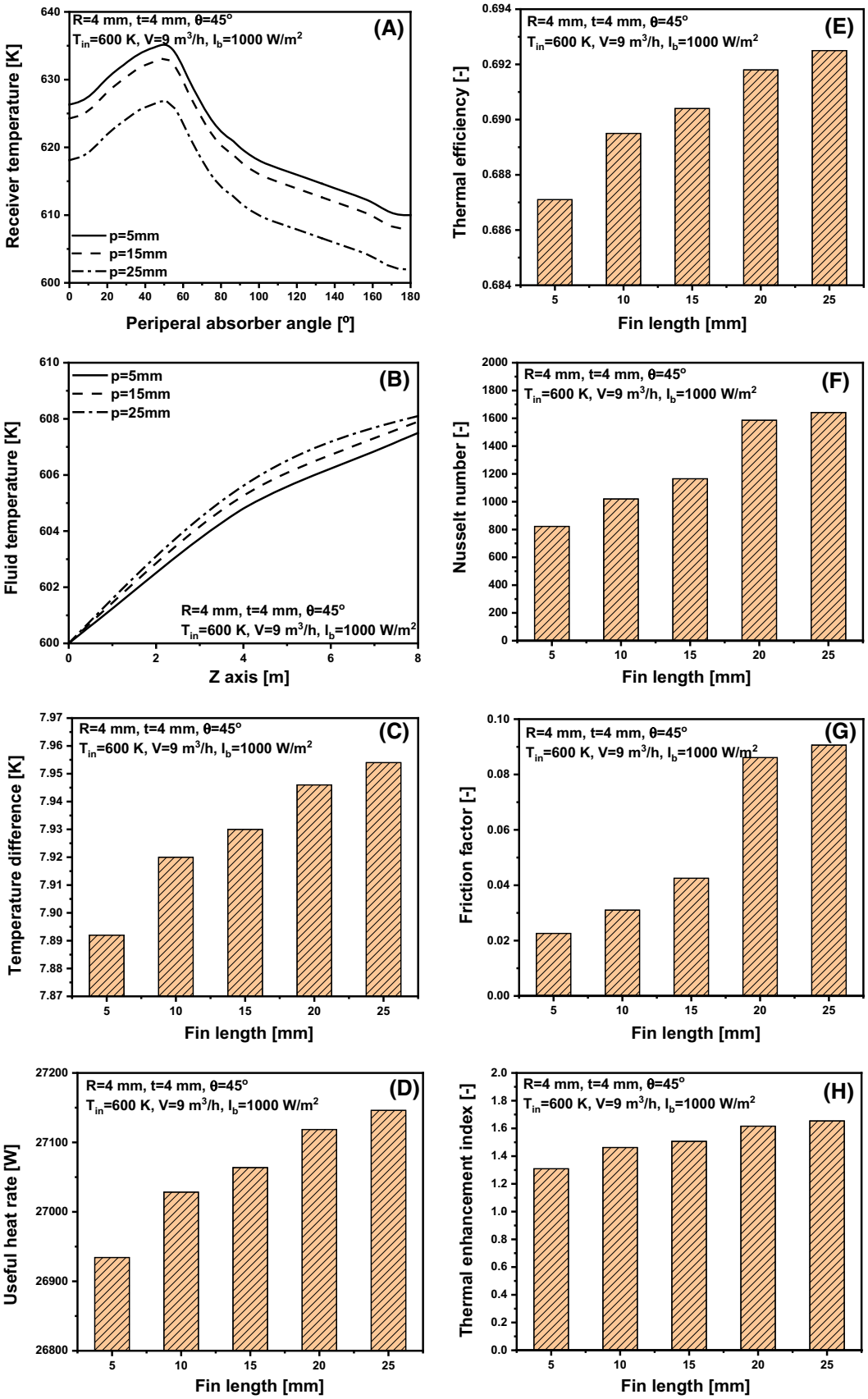


**Fig. 10** Effect of fin length on heat transfer characteristics

in the bottom of the absorber due to non-uniform heat flux distribution.

### 6.2 Effect of Fin Length

The effect of the fin length ($p$) on the performance characteristics of the parabolic trough concentrator is simulated with fin thickness and round edge radius of 4 mm and 4 mm, respectively. The angle between the fins, flow rate, inlet temperature and direct normal irradiance were kept constant at 45°, 9m$^3$/h, 600 K and 1000 W/m$^2$, respectively.

Figure 10a shows receiver temperature distribution values over the peripheral absorber angle for different lengths of fins. It is obvious that the receiver temperature decreases with increasing fin length. This is because of the higher turbulence and good mixing in the fluid flow are created when the fin length increases and then the useful heat and thermal efficiency increase, while the thermal losses decrease. The maximum receiver temperatures for fin length $p = 5$ mm and 25 mm are 635.24 and 626.917 K, respectively.

The relationship between the outlet fluid temperature value and different fin lengths is shown in Fig. 10b. The outlet temperature is directly proportional to the fin length due to its lower receiver temperature. The outlet temperatures for fin length, $p = 5$ mm and 25 mm are 607.892 and 607.954 K, respectively.

The temperature difference between the outlet and inlet fluid temperatures for different fin lengths is shown in Fig. 10c. Clearly, the temperature difference increases with the length of the fins. The temperature difference for the fin length of 20 mm is 7.946 K. Figure 10d presents useful heat rate values versus different fin lengths. It is evident that the increase in the length of the fins increases the heat transfer rate of the internal flow. This is due to the dual effects of increased surface area and higher turbulence in the fluid flow. Useful heat rate values range from 26,934 to 27,146 W for fin lengths from 5 to 25 mm.

The thermal efficiency as a function of fin length is shown in Fig. 10e. The greater the fin length, the higher the thermal efficiency because it has higher useful heat for the same direct solar irradiance. The thermal efficiency value for a fin length of 15 mm is 0.6904.

The Nusselt number as a function of fin length is shown in Fig. 10f, which proves that Nusselt number increases with the fin length. This is because higher fin length creates higher turbulence in the flow, which then enhances heat transfer inside the absorber tubes. The Nusselt number increases from 822 for the fin length of 5 mm to 1643 for the fin length of 25 mm. This means that the latter gives about twice the Nusselt number of the former.

Variation of the friction factor with fin length is shown in Fig. 10g. Due to the higher turbulence created in the fluid flow, the friction factor is higher with longer fin length. Obviously, a fin length of 25 mm produces a higher friction factor compared to a fin length of 5 mm. The friction factors are close to 0.0906 and 0.0226 for fin lengths of 25 mm and 5 mm, respectively.

The thermal enhancement index versus fin length is shown in Fig. 10h, which reveals that the thermal enhancement index

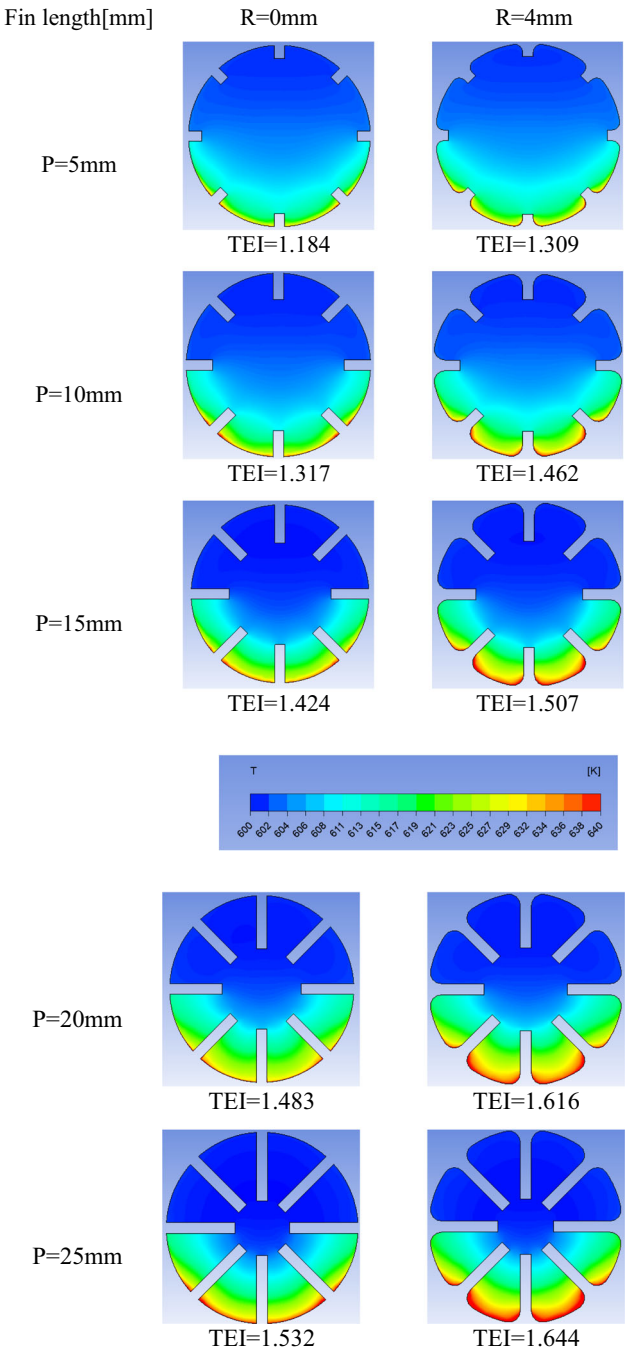


**Fig. 11** Temperature distribution contours in a mid-length of absorber tube for different fin length

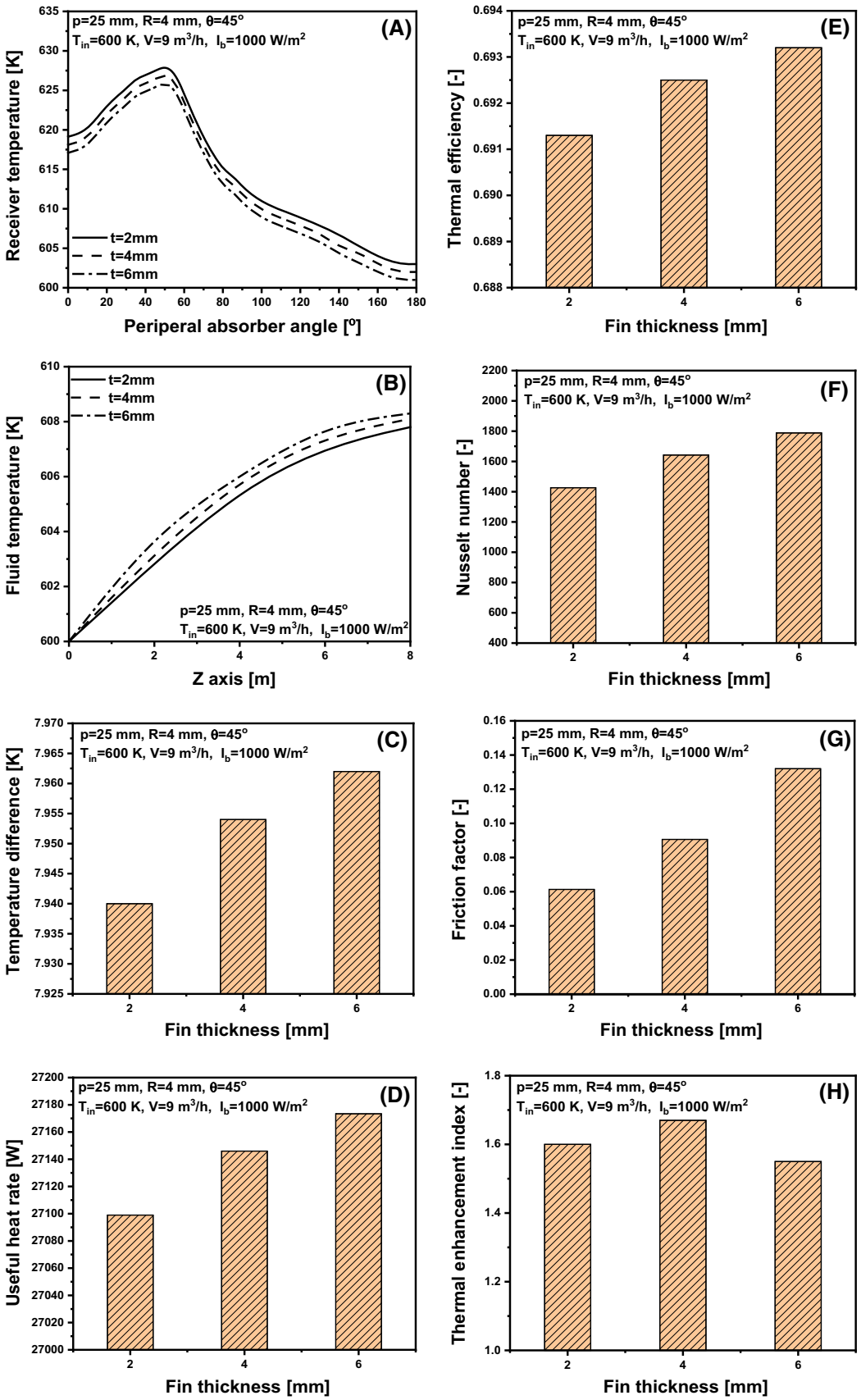


**Fig. 12** Effect of fin thickness on heat transfer characteristics

increases with the fin length. This is mainly due to the behavior of the Nusselt number and friction coefficient discussed earlier. The thermal enhancement index of the round edge fin with a length of 25 mm is nearly 25.6% higher than that of the round edge fin with a length of 5 mm.

Figure 11 shows the contours of the temperature distribution in the middle of the absorber tube length for rough conditions and different fin lengths (5, 10, 15, 20 and 25 mm). The thermal enhancement index of the round finned absorber is increased by 8.96% compared to the sharp edge with the fin length of 20 mm.

### 6.3 Effect of Fin Thickness

The effect of fin thickness on performance characteristics is conducted with the fin length of 25 mm, the radius of round edge of 4 mm, the inlet fluid temperature of 600 K, flow rate of 9 $m^3$/h and direct normal irradiance of 1000 W/$m^2$.

Figure 12a illustrates receiver temperature distribution values over peripheral absorber angles for different fin thicknesses. Higher fin thickness results in lower receiver temperature. When changing the fin thickness from 6 to 2 mm, the maximum temperature decreased from 627.958 to 625.875 K, respectively. As a result, the outlet temperature, differential temperature, effective heat consumption rate, and thermal efficiency were significantly improved (see Fig. 12b–e). Clearly, the outlet temperature, temperature difference, useful heat rate and thermal efficiency are directly proportional to the fin thickness. As the fin thickness increased from 2 to 6 mm, the temperature difference increased by nearly 0.3%, and the useful heat rate and thermal efficiency increased from 27,098 to 27,173 W and from 0.6913 to 0.6932, respectively.

Nusselt number as a function of fin thickness is shown in Fig. 12f, which reveals that the Nusselt number is directly proportional to the fin thickness. This is mainly due to higher turbulence in the flow. The fin thickness of 6 mm achieves the Nusselt number of 1788. Figure 12g shows the friction factor as a function of fin thickness. It can be observed that the coefficient of friction increases with increasing fin thickness, i.e., the coefficient of friction increases from 0.0613 to 0.132 when the fin thickness is changed from 2 to 6 mm.

Variation of thermal enhancement index with fin thickness is shown in Fig. 12h, which indicates that the fin thickness of 4 mm yields the highest thermal enhancement index of 1.644 among the investigated cases.

Figure 13 shows the temperature distribution contours of the mid-section of the absorber tube length with round edge fins compared to sharp edge fins with different fin thicknesses (2, 4 and 6 mm). At a fin thickness of 6 mm, the thermal enhancement index of the round edge fin is nearly 7.8% higher than that of the sharp edge fin.

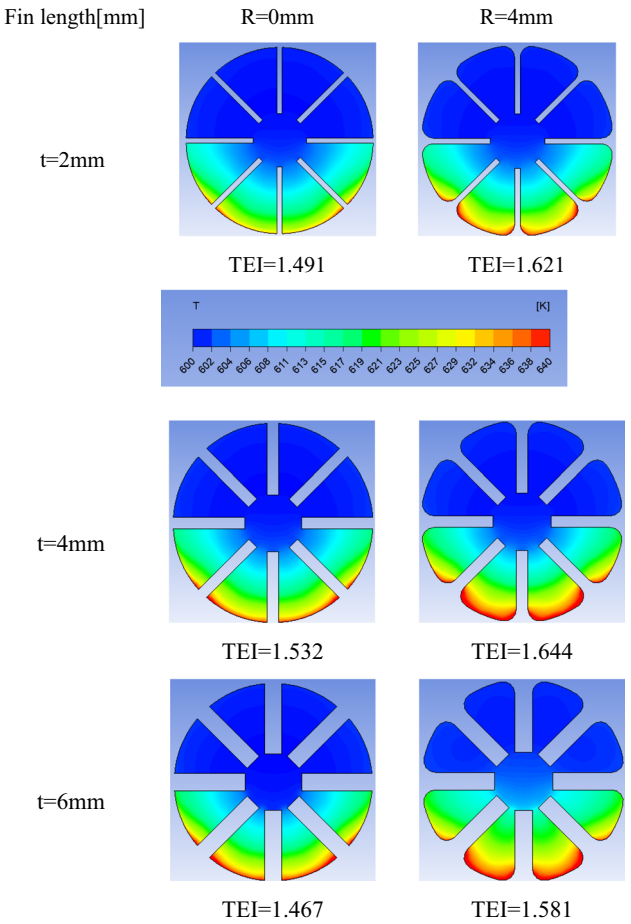


**Fig. 13** Temperature distribution contours in a mid-length of absorber tube for different fin thicknesses

### 6.4 Effect of Angle Between Fins

The effect of the angle ($\theta$) between the fins is investigated at 45° and 90° for fin lengths of 5 mm and 25 mm. The thickness and radius of the round edge fin were kept constant at 4 mm and 4 mm, respectively, the inlet fluid temperature, flow velocity and direct normal irradiance are kept constant.

The receiver temperature and outlet fluid temperature for absorber tubes with round and sharp edges as a function of the angle between the fins are plotted in Fig.14a, b for a fin length of 25 mm. Clearly, the receiver temperature is directly proportional, while the outlet fluid temperature is inversely proportional to the angle between the fins. This is because lower angle between fins increases the number of fins, which lead to higher turbulence in the fluid flow and improve the heat transfer in the absorber tube, then the receiver temperature decreases, and the outlet fluid temperature increases. As the angle between the fins was reduced from 90° to 45°, the maximum temperature of the receiver decreased from 629.76 to 626.64 K for rounded edges and from 630.8 to 627.68 K for sharp edges, respectively. As the angle between the fins

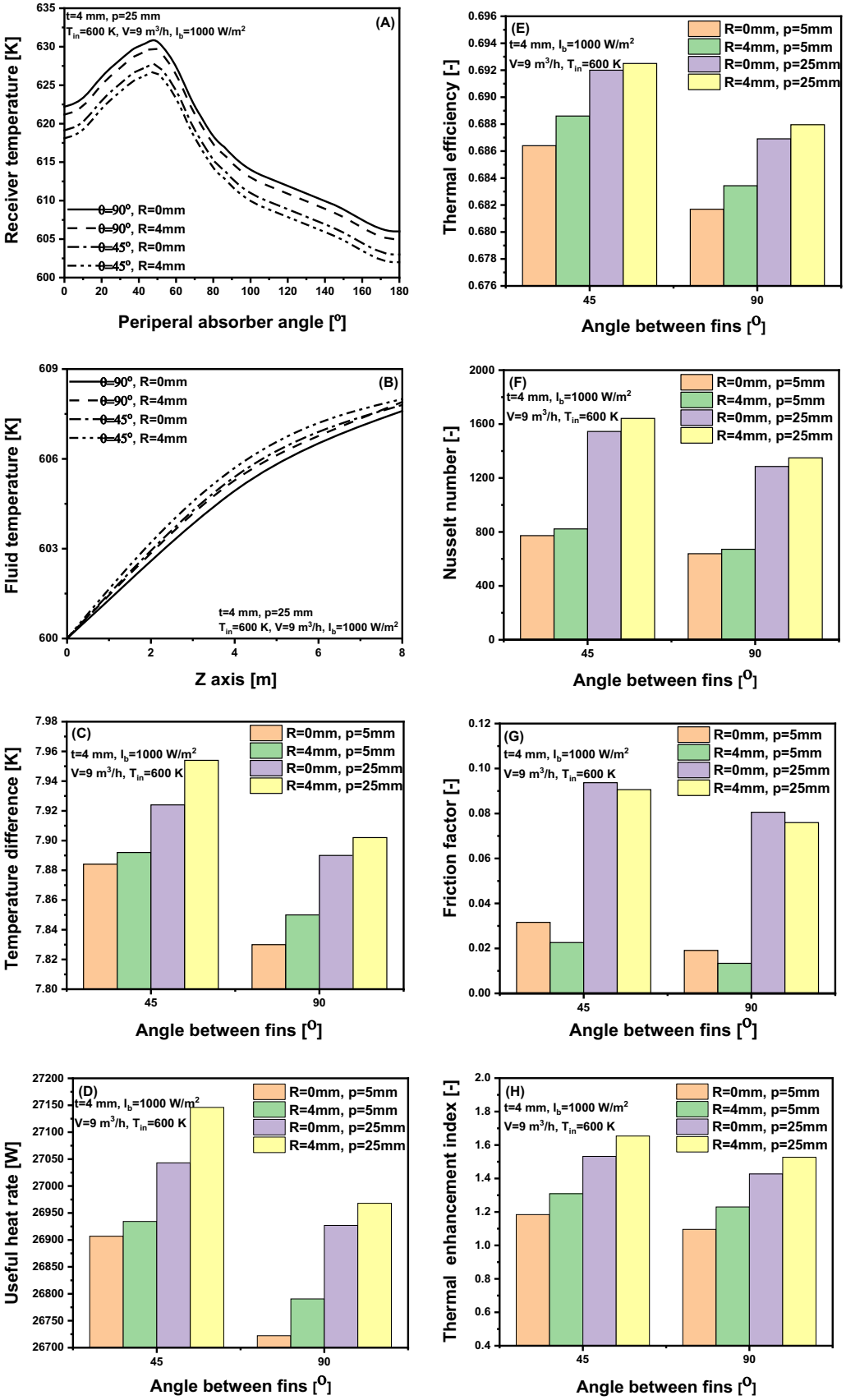


**Fig. 14** Effect of angle between fins on heat transfer characteristics

decreased from 90° to 45°, the temperature difference for the round and sharp-edged fins increased by nearly 0.7% and 0.43%, respectively.

Figure 14c–e illustrates the temperature difference, useful heat rate and thermal efficiency for absorber tubes with rounded and sharp edges as a function of angle between fins at different fin lengths of 5 and 25 mm. It is obvious that the temperature difference, useful heat rate and thermal efficiency of the absorber tube increase as the fin angle decreases. At a fin length of 5 mm, for varying angles from 90° to 45°, the temperature difference increases from 7.85 to 7.892 K for rounded edges and from 7.83 to 7.884 K for sharp edges, respectively. Useful heat rate increases from 26,790 to 26,934 W for rounded edges and from 26,722 W to 26,906 W for sharp edges, respectively. Also, thermal efficiency for rounded edges increases from 0.6834 to 0.688, and thermal efficiency for sharp edges increases from 0.6816 to 0.686, respectively, for varying angles from 90° to 45°.

Figure 14f presents the Nusselt numbers for different angles between fins for round and sharp-edged fins at fin lengths of 5 and 25 mm. This figure shows that at fixed fin length, the Nusselt number decreases with increasing angle between fins, while at the same angle between fins, the Nusselt number for round edge is higher than that of sharp edge. This is because larger angles between fins and rounded edges result in higher turbulence and better mixing than smaller angles between fins and sharp edges. The Nusselt number of 45° is nearly 21.7% higher than that of 90° at the rounded edge of the 25 mm fin length. At a 45° angle between fins with sharp edges, the Nusselt number for a 25 mm fin length is nearly 100% higher than that for a 5-mm fin length.

Figure 14g indicates the relationship between the friction factor and the angle between the fins for round and sharp-edged fins for fin lengths of 5 and 25 mm. At a fixed fin length, the friction factor is inversely proportional to the angle between the fins, which is due to the lower number of fins and less turbulence at higher angles. In the case of the same angle between fins, the friction factor of the round edge is lower than that of the sharp edge. Using sharp edges with a fin length of 5 mm, the friction factors at 45° and 90° are 0.0316 and 0.0191, respectively. The friction factors are 0.07593 and 0.01338 for round edge fins with 25-mm and 5-mm fin lengths at 90°, respectively.

Figure 14h shows the thermal enhancement index (TEI) as a function of the angle between the fins for round and sharp-edged fins at two fin lengths of 5 and 25 mm. This figure reveals that the best thermal enhancement index is achieved with a small angle between the fins, a larger fin length and round edge. At 45° angle and 25 mm fin length, the TEI for round and sharp-edged fins was 1.644 and 1.532, respectively.

Figure 15 shows the temperature distribution contours of the mid-section of the absorber tube length for tested cases with different fin angles of 45° and 90° and fin lengths of 5 mm and 25 mm. It is evident that when the fin angle is changed from 90° to 45°, the thermal enhancement index of the round edge fins with fin lengths of 5 mm and 25 mm increases by nearly 6.03% and 7.116%, respectively.

### 6.5 Effect of Operating Conditions

The effects of volume flow rate (V) in the range from 6 to 24 $m^3/h$, range of inlet fluid temperature (K) from 300 to 600 K and direct normal irradiance ($W/m^2$) changes from 500 to 1000 $W/m^2$ are investigated when the fin length, thickness, radius of round edge and angle between fins are kept constant.

The relationship between thermal efficiency and inlet fluid temperature at different volume flow rates is shown in Fig. 16a. Clearly, thermal efficiency is inversely proportional to inlet fluid temperature for all flow rate levels. This is because the higher inlet fluid temperature causes the heat absorbed by the working fluid to decrease and therefore the thermal efficiency is lower. When the inlet fluid temperature was increased from 300 to 600 K and the flow rate was 12 $m^3/h$, the thermal efficiency decreased by 6.944%. At higher flow rates, thermal efficiency increases due to greater heat absorption capacity. As the flow rate increased from 6 to 12 $m^3/h$, the thermal efficiency increased from 0.7164 to 0.7237 at an inlet fluid temperature of 500 K. Figure 16b shows variation of the thermal enhancement index with the inlet fluid temperature at different flow rates. Clearly, the thermal enhancement index increases with increasing inlet fluid temperature and decreasing flow rate. The thermal enhancement index values increase by 14.57% when inlet fluid temperature increases from 300 to 600 K at flow rate 9 $m^3/h$ and decrease by 11.63% as flow rate increases from 6 to 12 $m^3/h$ at the inlet fluid temperature of 600 K.

The thermal efficiency versus the direct normal irradiance at variety of flow rates is indicated in Fig. 16c, which reveals that both higher direct normal irradiance and flow velocity lead to higher thermal efficiency. Higher direct normal irradiance means this parameter ($\frac{T_{in}-T_{am}}{I_b}$) will reduce. The thermal efficiency increases from 0.684 to 0.693 for direct normal irradiance changes from 500 to 700 $W/m^2$ at flow rate 24 $m^3/h$ and increases from 0.681 to 0.689 for flow rate varies from 12 to 24 $m^3/h$ at direct normal irradiance 600 $W/m^2$. Figure 16d illustrates the thermal enhancement index versus direct normal irradiance at different flow rates. It can be observed that the thermal enhancement index is directly proportional to the direct normal irradiance and inversely proportional to the flow velocity. At a flow rate of 12 $m^3/h$, the thermal enhancement index increased from 1.265 to 1.359 as the direct normal irradiance varied from 500 to 700 $W/m^2$. At a direct normal irradiance of 700 $W/m^2$, the thermal enhancement index decreased from 1.359 to 1.153 when the flow rate was varied from 12 to 24 $m^3/h$.

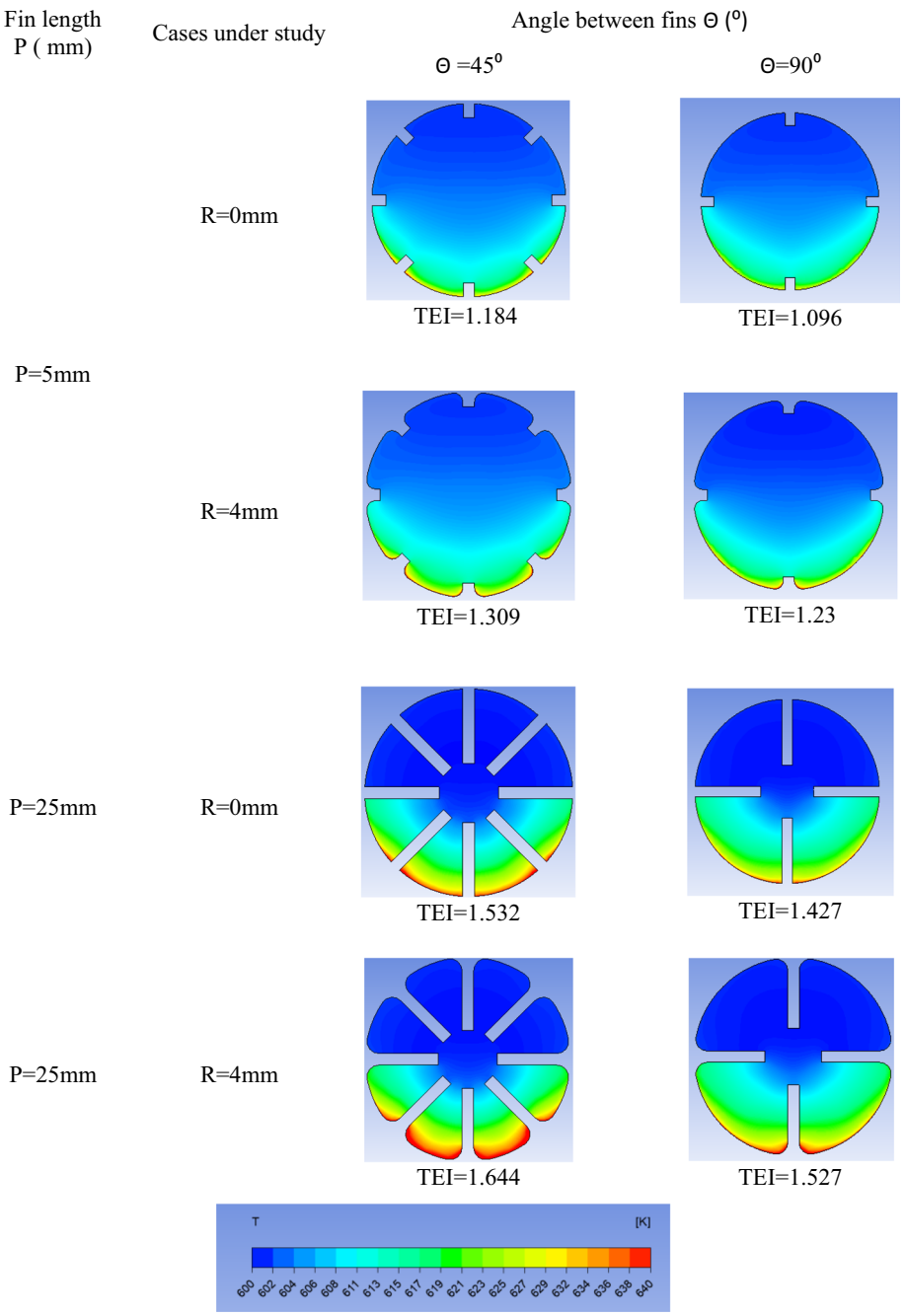


**Fig. 15** Temperature distribution contours in a mid-length of absorber tube for different angle between fins

## 6.6 Correlation of the Nusselt Number and Friction Factor

The relation between the Nusselt number or friction factor and both geometric and operating parameters is very useful for design engineers. Hence, this section aims to correlate the Nusselt number and friction factor with geometric and operational parameters based on the results reported in this study. These correlations can be used to provide a reliable model to assist system designers and operators in designing and evaluating the performance of round edge finned absorbers under different conditions. Thus, to generalize reported data in this study, the Nusselt number and friction factor are correlated with the relevant parameters [Reynolds number (Re), Prandtl number (Pr), dimensionless fin length ($p$/Dri), thickness ($t$/Dri), radius of round edge radii ($R$/Dri) and angle between fins ($\theta/2\ \pi$)] in the following forms:

$$Nu = A_0.\mathrm{Re}^{A_1}.\ \mathrm{Pr}^{A_2}.\left[1 + A_3.\left(\frac{R}{D_{ri}}\right)^{A_4}.\left(\frac{p}{D_{ri}}\right)^{A_5}.\left(\frac{t}{D_{ri}}\right)^{A_6}.\left(\frac{\theta}{2\pi}\right)^{A_7}\right. \quad (19)$$

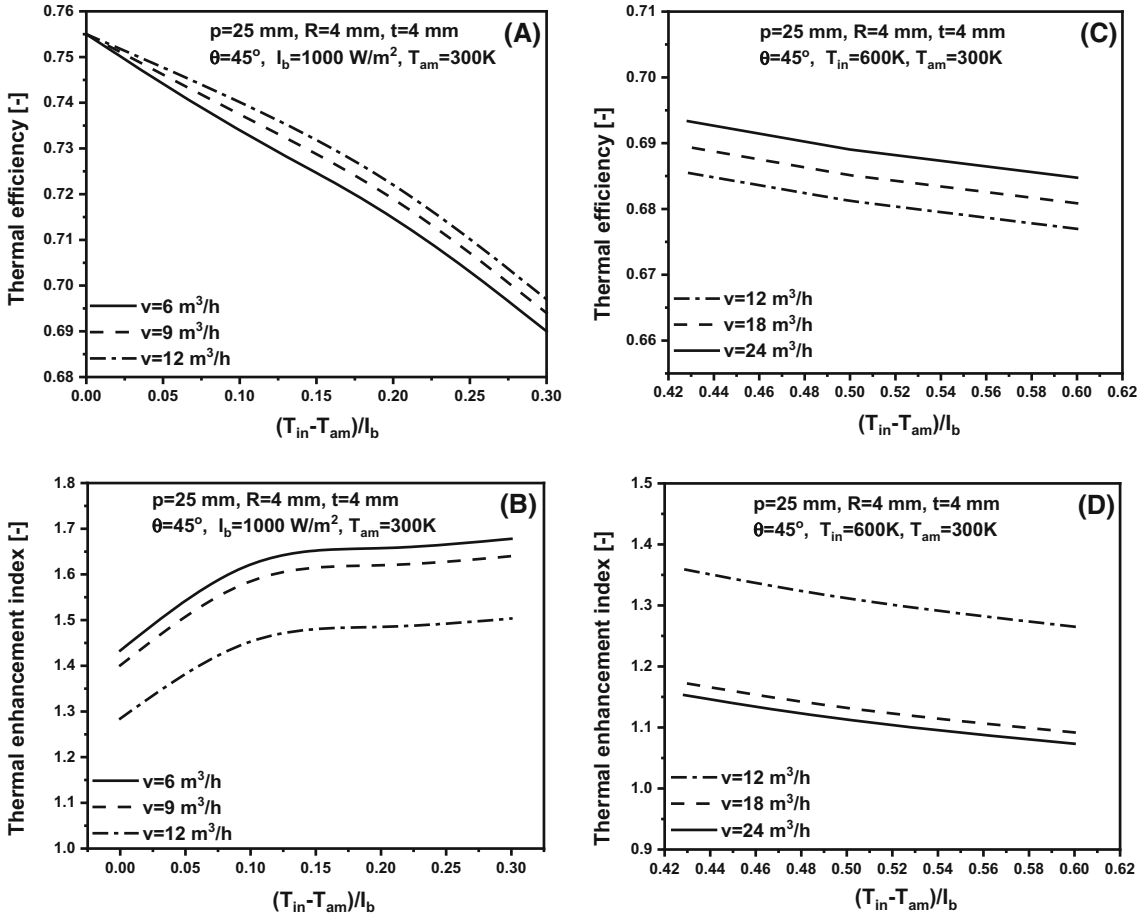


**Fig. 16** Effect of operating conditions on heat transfer characteristics

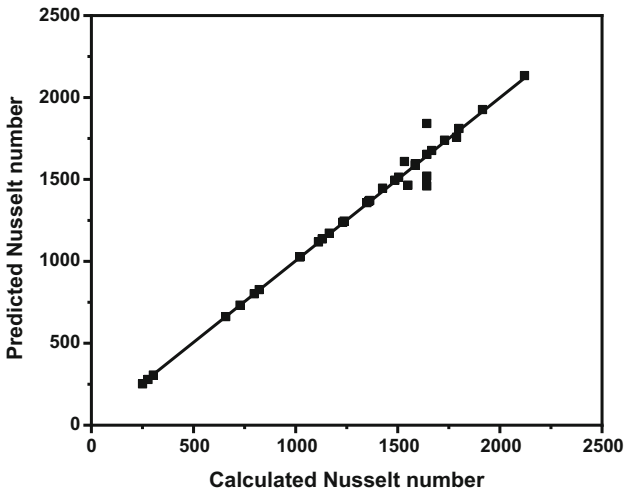


**Fig. 17** Predicted and calculated values of Nusselt number

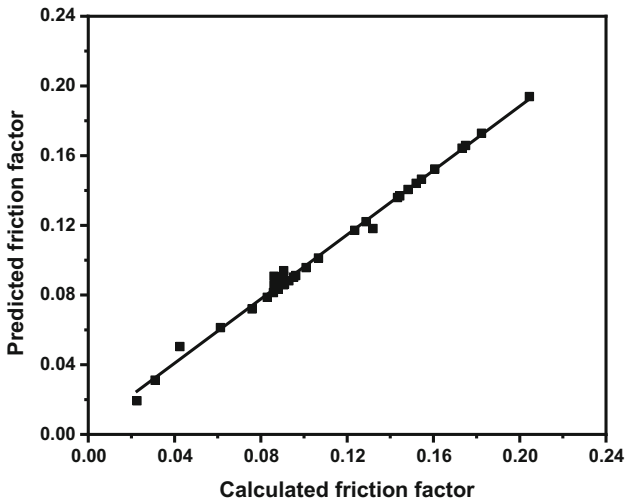


**Fig. 18** Predicted and calculated values of friction factor

$$f = \frac{B_0}{Re^{B_1}}.\left[1 + B_2.\left(\frac{R}{D_{ri}}\right)^{B_3}.\left(\frac{p}{D_{ri}}\right)^{B_4}.\left(\frac{t}{D_{ri}}\right)^{B_5}.\left(\frac{\theta}{2\pi}\right)^{B_6} . \exp\left(B_7.\frac{R}{D_{ri}}\right).\exp\left(B_8.\frac{p}{D_{ri}}\right).\exp\left(B_9.\frac{t}{D_{ri}}\right).\exp\left(B_{10}.\frac{\theta}{D_{ri}}\right)\right] \quad (20)$$

where $A_0$, $A_1$, $A_2$, $A_3$, $A_4$, $A_5$, $A_6$ and $A_7$ are numerical constants in Eq. (19) with corresponding values of 1.1438, 0.8405, 0.2657, 0.8319, 0.4751, 0.1958 and − 0.2037,

respectively. In addition, $B_0$, $B_1$, $B_2$, $B_3$, $B_4$, $B_5$, $B_6$, $B_7$, $B_8$, $B_9$ and $B_{10}$ are numerical constants in Eq. (20) whose corresponding values are 1.616, 0.189, − 0.758, 1.1796, 0.808 and − 0.266, respectively. The above equations relate the Nusselt number and friction coefficient to the relevant parameters with multiple correlation coefficients ($R2$) of 0.993 and 0.973, respectively. It may be noted that these correlations are valid for fin length ($p = 5$, 10, 15, 20 and 25 mm), fin thickness ($t = 2$, 4 and 6 mm), round edge radii ($R = 2$, 3 and 4 mm), angle between fins ($\theta = 45°$, 90°), inlet fluid temperature (300–600 K), direct normal irradiance (500–1000 W/m2) and fluid flow rate (6–24 m3/h).

Figures 17, 18) compare the predicted and simulation data of the Nusselt number and the friction factor. This comparison confirms that the predicted data for Nusselt number and coefficient of friction are accurate, so Eqs. (19) and (20) can yield reliable data.

## 7 Conclusions

The objective of the present research is to examine the use of rounded edges at the bottom of the fins in the absorber of the LS-2 parabolic trough collector. The fins are available in lengths of 5, 10, 15, 20 and 25 mm, thicknesses of 2, 4 and 6 mm, different radii of 2, 3 and 4 mm, and angles between fins of 45° and 90°. Computational fluid dynamics (CFD) with UDF code was used to develop a simulation model of the fin configurations under consideration. Then, the simulation model results are verified using the literature data.

All fin configurations are examined under inlet temperatures in the range of 300: 600 K, volume flow rates in the range of 6:24 $m^3$/h and direct normal irradiance in the range of 500: 1000 W/$m^2$. The main criteria to decide the best design are the increase in the friction factor, the Nusselt number enhancement and the thermal enhancement index. The best design for this study was investigated for inlet temperatures of 300–600 K, flow rates of 6–24 $m^3$/h, and direct normal irradiance of 500–1000 W/$m^2$. Based on the results of the report, the following conclusions can be drawn:

- The thermal efficiency of rounded fins with a radius of 4 mm inside the absorber is 1.363% higher than that of a smooth case when the fin length and thickness are 20 mm and 4 mm.
- The Nusselt number at 25-mm fin length is 1.997 times higher than at 5-mm fin length, 4-mm fin thickness and 4-mm edge radius.
- Increasing the fin thickness from 2 to 6 mm increases the Nusselt number by a factor of 1.254 at a fin length of 25 mm and a round edge radius of 4 mm.
- The increase in fin length and thickness enhanced heat transfer and increased pressure loss, but a fin thickness of 6 mm resulted in the lowest thermal enhancement index.
- At a fin length of 25 mm, the thermal enhancement index values at the angles between the fins of 45° and 90° are 1.644 and 1.527, respectively, for the round edge and are 1.532 and 1.427, respectively, for the sharp edge.
- According to the highest thermal enhancement index value of 1.644, the best case is that the fin length is 25 mm, the thickness is 4 mm, the radius of the round edge is 4 mm, and the angle between the fins is 45°.

**Funding** Open access funding provided by The Science, Technology & Innovation Funding Authority (STDF) in cooperation with The Egyptian Knowledge Bank (EKB).



## References

1. Goel, A.; Manik, G.; Verma, O.P.: Designing a robust analytical model of a parabolic trough solar collector through in-depth analysis of convective heat transfers. Arab. J. Sci. Eng. (2022). https://doi.org/10.1007/s13369-021-06473-y
2. Mousa, M.H.; Miljkovic, N.; Nawaz, K.: Review of heat transfer enhancement techniques for single phase flows. Renew. Sust. Energ. Rev (2021). https://doi.org/10.1016/j.rser.2020.110566
3. Goshayeshi, H.R.; Safaei, M.R.: Effect of absorber plate surface shape and glass cover inclination angle on the performance of a passive solar still. Int. J. Numer. Meth. Heat Fluid Flow (2020). https://doi.org/10.1108/HFF-01-2019-0018
4. Jathar, L.D.; Ganesan, S.; Shahapurkar Soudagar, M.E.M.; Mujtaba, M.A.; Anqi, A.E.; Farooq, M.; Khidmatgar, A.; Goodarzi, M.; Safaei, M.R.: Effect of various factors and diverse approaches to enhance the performance of solar stills: a comprehensive review. J. Therm. Anal. Calorim. (2022). https://doi.org/10.1007/s10973-021-10826-y
5. Maithani, R.; Kumar, A.; Zadeh, P.G.; Safaei, M.R.; Gholamalizadeh, E.: Empirical correlations development for heat transfer and friction factor of a solar rectangular air passage with spherical-shaped turbulence promoters. J. Therm. Anal. Calorim. (2019). https://doi.org/10.1007/s10973-019-08551-8
6. Abuşka, M.; Akgül, M.B.: Experimental study on thermal performance of a novel solar air collector having conical springs on absorber plate. Arab. J. Sci. Eng. (2016). https://doi.org/10.1007/s13369-016-2177-4

7. Nima, M.A.; Ali, A.M.: Effect of metal foam insertion on thermal performance of flat-plate water solar collector under iraqi climate conditions. Arab. J. Sci. Eng. (2017). https://doi.org/10.1007/s13369-017-2683-z
8. Aldulaimi, R.K.M.: An innovative receiver design for a parabolic trough solar collector using overlapped and reverse flow: an experimental study. Arab. J. Sci. Eng. (2019). https://doi.org/10.1007/s13369-019-03832-8
9. Kurşun, B.: Thermal performance assessment of internal longitudinal fins with sinusoidal lateral surfaces in parabolic trough receiver tubes. Renew. energy. (2019). https://doi.org/10.1016/j.renene.2019.03.106
10. Bellos, E.; Tzivanidis, C.; Tsimpoukis, D.: Multi-criteria evaluation of parabolic trough collector with internally finned absorbers. Appl. Energy. (2017). https://doi.org/10.1016/j.apenergy.2017.07.141
11. Bellos, E.; Tzivanidis, C.; Daniil, I.; Antonopoulos, K.A.: The impact of internal longitudinal fins in parabolic trough collectors operating with gases. Energy Convers. Manag (2017). https://doi.org/10.1016/j.enconman.2016.12.057
12. Bellos, E.; Tzivanidis, C.; Tsimpoukis, D.: Optimum number of internal fins in parabolic trough collectors. Appl. Therm. Eng. (2018). https://doi.org/10.1016/j.applthermaleng.2018.04.037
13. Goel, V.; Hans, V.S.; Singh, S.; Kumar, R.; Pathak, S.K.; Singla, M.; Saini, R.P.: A comprehensive study on the progressive development and applications of solar air heaters. Sol. Energy (2021). https://doi.org/10.1016/j.solener.2021.07.040
14. Nemś, M.; Kasperski, J.: Experimental investigation of concentrated solar air-heater with internal multiple-fin array. Renew. Energy (2016). https://doi.org/10.1016/j.renene.2016.06.038
15. Amina, B.; Miloud, A.; Samir, L.; Abdelylah, B.; Solano, J.P.: Heat transfer enhancement in a parabolic trough solar receiver using longitudinal fins and nanofluids. J. Therm. Sci. (2016). https://doi.org/10.1007/s11630-016-0878-3
16. Laaraba, A.; Mebarki, G.: Enhancing thermal performance of a parabolic trough collector with inserting longitudinal fins in the down half of the receiver tube. J. Therm. Sci. (2020). https://doi.org/10.1007/s11630-020-1256-8
17. Zhao, Z.; Bai, F.; Zhang, X.; Wang, Z.: Experimental study of pin finned receiver tubes for a parabolic trough solar air collector. Sol. Energy (2020). https://doi.org/10.1016/j.solener.2020.06.070
18. Gong, X.; Wang, F.; Wang, H.; Tan, J.; Lai, Q.; Han, H.: Heat transfer enhancement analysis of tube receiver for parabolic trough solar collector with pin fin arrays inserting. Sol. Energy (2017). https://doi.org/10.1016/j.solener.2017.01.020
19. Allam, M.; Tawfik, M.; Bekheit, M.; El-Negiry, E.: Heat transfer enhancement in parabolic trough receivers using inserts: a review. Sustain. Energy Technol. Assess. (2021). https://doi.org/10.1016/j.seta.2021.101671
20. Huang, Z.; Yu, G.L.; Li, Z.Y.; Tao, W.Q.: Numerical study on heat transfer enhancement in a receiver tube of parabolic trough solar collector with dimples, protrusions and helical fins. Energy Procedia (2015). https://doi.org/10.1016/j.egypro.2015.03.149
21. Kalidasan, B.; Shankar, R.; Srinivas, T.: Absorber tube with internal hinged blades for solar parabolic trough collector. Energy Procedia (2016). https://doi.org/10.1016/j.egypro.2016.11.213
22. Huang, Z.; Li, Z.Y.; Yu, G.L.; Tao, W.Q.: Numerical investigations on fully-developed mixed turbulent convection in dimpled parabolic trough receivertubes. Appl. Therm. Eng. (2017). https://doi.org/10.1016/j.applthermaleng.2016.10.012
23. Bellos, E.; Tzivanidis, C.; Antonopoulos, K.A.; Gkinis, G.: Thermal enhancement of solar parabolic trough collectors by using nanofluids and converging-diverging absorber tube. Renew. Energy. (2016). https://doi.org/10.1016/j.renene.2016.03.062
24. Demagh, Y.; Hachicha, A.A.; Benmoussa, H.; Kabar, Y.: Numerical investigation of a novel sinusoidal tube receiver for parabolic trough technology. Appl. Energy (2018). https://doi.org/10.1016/j.apenergy.2018.02.177
25. Fuqiang, W.; Zhexiang, T.; Xiangtao, G.; Jianyu, T.; Huaizhi, H.; Bingxi, L.: Heat transfer performance enhancement and thermal strain restrain of tube receiver for parabolic trough solar collector by using asymmetric outward convex corrugatedtube. Energy (2016). https://doi.org/10.1016/j.energy.2016.08.013
26. Mahmoud, M.S.; Abbas, A.; Khudheyer, A.F.: Solar parabolic trough collector tube heat transfer analysis with internal conical pin fins. J. Green Eng. (2020). https://doi.org/10.1016/j.solener.2017.01.020
27. Okonkwo, E.C.; Abid, M.; Ratlamwala, T.A.: Effects of synthetic oil nanofluids and absorber geometries on the exergetic performance of the parabolic trough collector. Int. J. Energy Res. (2018). https://doi.org/10.1002/er.4099
28. Okonkwo, E.C.; Abid, M.; Ratlamwala, T.A.: Comparative study of heat transfer enhancement in parabolic trough collector based on modified absorbergeometry. J. EnergyEng. (2019). https://doi.org/10.1061/(ASCE)EY.1943-7897.0000602
29. Bellos, E.; Tzivanidis, C.: Enhancing the performance of evacuated and non-evacuated parabolic trough collectors using twisted tape inserts, perforated plate inserts and internally finned absorber. Energies (2018). https://doi.org/10.3390/en11051129
30. Khan, M.S.; Yan, M.; Ali, H.M.; Amber, K.P.; Bashir, M.A.; Akbar, B.; Javed, S.: Comparative performance assessment of different absorber tube geometries for parabolic trough solar collector usingnanofluid. J. Therm. Anal. Calorim. (2020). https://doi.org/10.1007/s10973-020-09590-2
31. Sarafraz, M.M.; Safaei, M.R.: Diurnal thermal evaluation of an evacuated tube solar collector (ETSC) charged with graphene nanoplatelets-methanol nano-suspension. Renew. Energy (2019). https://doi.org/10.1016/j.renene.2019.04.091
32. Peng, Y.; Zahedidastjerdi, A.; Abdollahi, A.; Amindoust, A.; Bahrami, M.; Karimipour, A.; Goodarzi, M.: Investigation of energy performance in a U-shaped evacuated solar tube collector using oxide added nanoparticles through the emitter, absorber and transmittal environments via discrete ordinates radiation method. J. Therm. Anal. Calorim. (2020). https://doi.org/10.1007/s10973-019-08684-w
33. Sarafraz, M.M.; Tlili, I.; Tian, Z.; Bakouri, M.; Safaei, M.R.; Goodarzi, M.: Thermal evaluation of graphene nanoplatelets nanofluid in a fast-responding HP with the potential use in solar systems in smart cities. Appl. Sci. (2019). https://doi.org/10.3390/app9102101
34. Jamshed, W.; Devi, S.S.U.; Goodarzi, M.; Prakash, M.; Nisar, K.S.; Zakarya, M.; Abdel-Aty, A.-H.: Evaluating the unsteady Casson nanofluid over a stretching sheet with solar thermal radiation: an optimal case study. Case Stud. Therm. Eng. (2021). https://doi.org/10.1016/j.csite.2021.101160
35. Safaei, M.R.; Goshayeshi, H.R.; Chaer, I.: Solar still efficiency enhancement by using graphene oxide/paraffin nano-PCM. Energies (2019). https://doi.org/10.3390/en12102002
36. Khosravi, R.; Rabiei, S.; Khaki, M.; Safaei, M.R.; Goodarzi, M.: Entropy generation of graphene–platinum hybrid nanofluid flow through a wavy cylindrical microchannel solar receiver by using neural networks. J. Therm. Anal. Calorim. (2021). https://doi.org/10.1007/s10973-021-10828-w
37. Sarafraz, M.M.; Tlili, I.; Tian, Z.; Bakouri, M.; Safaei, M.R.: Smart optimization of a thermosyphon heat pipe for an evacuated tube solar collector using response surface methodology (RSM). Phys. A Stat. Mech. Appl. (2019). https://doi.org/10.1016/j.physa.2019.122146
38. Sarafraz, M.M.; Tlili, I.; Abdul Baseer, M.; Safaei, M.R.: Potential of solar collectors for clean thermal energy production in

smart cities using nanofluids: experimental assessment and efficiency improvement. Appl. Sci. (2019). https://doi.org/10.3390/app9091877
39. Olia, H.; Torabi, M.; Bahiraei, M.; Ahmadi, M.H.; Goodarzi, M.; Safaei, M.R.: Application of nanofluids in thermal performance enhancement of parabolic trough solar collector: state-of-the-art. Appl. Sci (2019). https://doi.org/10.3390/app9030463
40. Saleh, B.; Sundar, L.S.; Aly, A.A.; Ramana, E.V.; Sharma, K.V.; Afzal, A.; Abdelrhman, Y.; Sousa, A.C.M.: The combined effect of $Al_2O_3$ nanofluid and coiled wire inserts in a flat-plate solar collector on heat transfer, thermal efficiency and environmental $CO_2$ characteristics. Arab. J. Sci. Eng. (2022). https://doi.org/10.1007/s13369-021-06478-7
41. Bellos, E.; Tzivanidis, C.; Tsimpoukis, D.: Enhancing the performance of parabolic trough collectors using nanofluids and turbulators. Renew. Sustain. Energy Rev. (2018). https://doi.org/10.1016/j.rser.2018.03.091
42. Bellos, E.; Daniil, I.; Tzivanidis, C.: Multiple cylindrical inserts for parabolic trough solar collector. Appl. Therm. Eng. (2018). https://doi.org/10.1016/j.applthermaleng.2018.07.086
43. Akbarzadeh, S.; Valipour, M.S.: Heat transfer enhancement in parabolic trough collectors: a comprehensive review. Renew. Sustain. Energy Rev. (2018). https://doi.org/10.1016/j.rser.2018.04.093
44. Ahmed, K.A.; Natarajan, E.: Thermal performance enhancement in a parabolic trough receiver tube with internal toroidal rings: a numerical investigation. Appl. Therm. Eng. (2019). https://doi.org/10.1016/j.applthermaleng.2019.114224
45. Vishwakarma, S.; Debnath, K.; Debnath, B.K.: Thermal performance study of helically grooved absorber tubes for parabolic trough solar collector. In: ASME Power Conference (Vol. 51395, p. V001T06A009). American Society of Mechanical Engineers.(2018,June). https://doi.org/10.1115/POWER2018-7270
46. Amani, K.; Ebrahimpour, M.; Akbarzadeh, S.; Valipour, M.S.: The utilization of conical strip inserts in a parabolic trough collector. J. Therm. Anal. Calorim. (2020). https://doi.org/10.1007/s10973-019-09233-1
47. Okonkwo, E.C.; Abid, M.; Ratlamwala, T.A.: Numerical analysis of heat transfer enhancement in a parabolic trough collector based on geometry modifications and working fluid usage. J. Sol. Energy Eng (2018). https://doi.org/10.1115/1.4040076
48. Singh, S.; Dhiman, P.: Thermal performance analysis of a rectangular longitudinal finned solar air heater with semicircular absorber plate. J. Sol. Energy Eng. (2016). https://doi.org/10.1115/14032010
49. Kalidasan, B.; Shankar, R.; Srinivas, T.: Absorber tube with internal pin-fins for solar parabolic trough collector. In: MATEC Web of Conferences (Vol. 55, p. 06004). EDP Sciences, (2016). https://doi.org/10.1051/matecconf/20165506004
50. Ganga, A.; Jacob, T.: Heat transfer enhancement analysis of solar parabolic trough collector tube with pin fins. Heat Transf. (2019).
51. Biswakarma, S.; Roy, S.; Das, B.; Debnath, B.K.: Performance analysis of internally helically v-grooved absorber tubes using nanofluid. Thermal Sci. Eng. Progress (2020). https://doi.org/10.1016/j.tsep.2020.100538
52. Zaboli, M.; Mousavi Ajarostaghi, S.S.; Saedodin, S.; Saffari Pour, M.: Thermal performance enhancement using absorber tube with inner helical axial fins in a parabolic trough solar collector. Appl. Sci. (2021). https://doi.org/10.3390/app11167423
53. Nnamchi, S.N.; Nnamchi, O.A.; Onuorah, M.O.; Nkurunziza, K.O.; Ismael, S.A.: Design and simulation of air-solar-finned reheating unit: an innovative design of a parabolic trough solar collector. Cogent Eng. (2020). https://doi.org/10.1080/23311916.2020.1793453
54. Sharma, M.; Jilte, R.: A review on passive methods for thermal performance enhancement in parabolic trough solar collectors. Int. J. Energy Res. (2021). https://doi.org/10.1002/er.6212
55. Bellos, E.; Tzivanidis, C.; Tsimpoukis, D.: Thermal enhancement of parabolic trough collector with internally finned absorbers. Sol. Energy (2017). https://doi.org/10.1016/j.solener.2017.08.067
56. Behar, O.; Khellaf, A.; Mohammedi, K.: A novel parabolic trough solar collector model–validation with experimental data and comparison to engineering equation solver (EES). Energy Convers. Manag. (2015). https://doi.org/10.1016/j.enconman.2015.09.045
57. Dudley, V. E.; Kolb, G. J.; Mahoney, A. R.; Mancini, T. R.; Matthews, C. W.; Sloan, M. I. C. H. A. E. L.; Kearney, D.: Test results: SEGS LS-2 solar collector (No. SAND94–1884). Sandia National Lab. (SNL-NM), Albuquerque, NM (UnitedStates), (1994).https://doi.org/10.2172/70756
58. Ansys Inc., "ANSYS FLUENT 14.0 Theory Guide," (2011).